

**EFFECT OF TEST CONDITIONS AND SAMPLE CONFIGURATION ON THE
AMTEC ELECTRODE/ELECTROLYTE CHARACTERISTICS
MEASUREMENTS IN THE SODIUM EXPOSURE TEST CELL EXPERIMENT**

A Thesis

by

ULUGHBEK BAKHADIROVICH AZIMOV

Submitted to the Office of Graduate Studies of
Texas A&M University
in partial fulfillment of the requirements for the degree of

MASTER OF SCIENCE

December 2001

Major Subject: Mechanical Engineering

**EFFECT OF TEST CONDITIONS AND SAMPLE CONFIGURATION ON THE
AMTEC ELECTRODE/ELECTROLYTE CHARACTERISTICS
MEASUREMENTS IN THE SODIUM EXPOSURE TEST CELL EXPERIMENT**

A Thesis

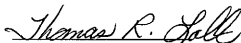
by

ULUGHBEK BAKHADIROVICH AZIMOV

Submitted to the Office of Graduate Studies of
Texas A&M University
in partial fulfillment of the requirements for the degree of

MASTER OF SCIENCE

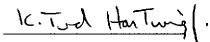
Approved as to style and content by:



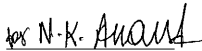
Thomas R. Lalk
(Chair of Committee)



Michael Schuller
(Member)



Ted Hartwig
(Member)



John Weese
(Interim Head of Department)

December 2001

Major Subject: Mechanical Engineering

ABSTRACT

Effect of Test Conditions and Sample Configuration on the AMTEC
Electrode/Electrolyte Characteristics Measurements in the Sodium Exposure Test Cell
Experiment.

(December 2001)

Ulughbek Bakhadirovich Azimov, B.S., Andijan Technical University
Chair of Advisory Committee: Dr. Thomas R. Lalk

An experimental investigation was conducted to determine the effect of test conditions and sample configuration on the AMTEC electrode/electrolyte characteristic measurements in a Sodium Exposure Test Cell (SETC). The effect of test conditions was determined by identifying the accurate correlation between sodium temperature and vapor pressure in the correct temperature range for the SETC. In addition, temperature distribution in the sodium source in SETC was determined. A correlation was identified that accurately predicted the relationship between the sodium vapor source temperature and the vapor pressure. A means to maintain the uniformity of the temperature across the electrode/electrolyte sample and in the sodium vapor source was determined.

Two electrode/electrolyte configurations (tube and disk) were tested to determine if there was a difference in the characteristics determined from the measurements. It was demonstrated that the configuration of the sample had little effect (about 15%) on the measurements at typical AMTEC operating temperatures. Electrochemical Impedance Spectroscopy (EIS) and controlled potential current-voltage curves (*i*V curves) techniques were used to determine these characteristics.

DEDICATION

I dedicate this work to my grandfather, Dr. Yunus Kadirov, for being an inspirational example to me. His constant encouragement has been a driving force helping me to reach for my dreams. Thank you.

ACKNOWLEDGEMENTS

I thank the government of Uzbekistan and the “UMID” Presidential Foundation for giving me the opportunity to succeed in this life for the sake of the UZBEK nation.

I would like to thank my advisor and committee chairman, Dr. Thomas R. Lalk, for his guidance, support, and attitude to make things work. I express my deepest gratitude to him for teaching me how to write effectively, how to ask the right questions, and most importantly, how to think on my feet. I am indebted to Dr. Lalk for helping me with all my professional and personal problems.

I thank Dr. Michael Schuller, an associate director of the Center for Space Power and my mentor, for teaching me techniques of electrochemistry and experimental setup; for his patience and encouragement during my experiments in his laboratory, in particular, for identifying my mistakes and giving the possible alternatives to correct them. Dr. Schuller has been a source of unbounded knowledge, helping me to gain a deeper understanding of my research. I thank him for giving effective ideas for my research and for being with me all the way from the beginning to the end, including experiments, discussions of results and preparation of my thesis.

I thank Dr. Ted K. Hartwig for serving on my graduate committee and for giving me his valuable suggestions.

I appreciate Yuyan Guo, Ph.D student, for helping me to set up lab experiments and with whom I am honored to have worked.

My special gratitude is to Cliff Spence, my officemate, for sharing his knowledge with me and for his continuous support.

I would like to give my deepest appreciation to Mrs. Violetta Cook, Director of Sponsored Student Programs, for her willingness to understand the problems of international students and for her invaluable support when I faced difficulties.

Finally, I would like to thank my family for their love, support and patience being apart for the considerable period of time. I am grateful for the support, care, and fellowship from my wife, Inara, who has been the beauty of life that has sustained me and given me a positive vision.

TABLE OF CONTENTS

	Page
ABSTRACT.....	iii
DEDICATION.....	iv
ACKNOWLEDGEMENTS.....	v
TABLE OF CONTENTS.....	vii
LIST OF TABLES.....	ix
LIST OF FIGURES.....	x
CHAPTER I INTRODUCTION.....	1
1.1. Motivation for Research.....	1
1.2. Description of AMTEC Operation.....	2
1.3. Objectives of Research and Format of Thesis.....	7
CHAPTER II LITERATURE REVIEW.....	10
2.1. Description of the Processes in AMTEC Electrode/Electrolyte Assembly.....	10
2.1.1. Elements of an Electrode/Electrolyte Assembly.....	10
2.1.2. Physical Processes in the Electrode/Electrolyte Assembly.....	12
2.1.2.1. Sodium Gas Diffusion.....	12
2.1.2.2. Electrochemical Reactions.....	13
2.1.2.3. Ion Transfer.....	13
2.1.2.4. Electron Transfer.....	14
2.1.3. Electrical Production.....	14
2.1.3.1. Theoretical Cell Potential.....	15
2.1.3.2. Overpotential.....	18
2.1.3.3. Limiting Current.....	22
2.2. β'' -alumina Solid Electrolyte.....	22
2.2.1. Overview of β'' -alumina Group Ceramics.....	23
2.2.2. Structure of β -alumina Group Oxides.....	23
2.2.3. Ionic Conductivity and Diffusion Mechanisms in β'' -alumina.....	26
2.2.4. Composition and Phase Relationships of β'' -alumina.....	30
2.3. Performance Characteristics of AMTEC Electrode/Electrolyte Assembly Components.....	31
2.3.1. Performance Degradation of β'' -alumina Solid Electrolyte at AMTEC Operating Conditions.....	31
2.3.2. Performance Characterization of AMTEC Electrodes.....	34
2.3.2.1. AMTEC Electrode Requirements.....	34
2.3.2.2. AMTEC Electrode Characteristics.....	35
2.3.2.3. Sodium Transport Modes in AMTEC Electrodes.....	37

	Page
2.3.2.4. Performance Optimization of AMTEC Electrodes.....	38
CHAPTER III APPARATUS AND EXPERIMENTAL PROCEDURE.....	41
3.1. Apparatus.....	41
3.1.1. The Sodium Exposure Test Cell.....	41
3.1.1.1. Performance Optimization of Sodium Exposure Test Cell.....	45
3.1.1.2. Classification of Functions in the SETC Experiment.....	51
3.2. Analysis of Tasks.....	55
3.2.1. Effect of Sodium Vapor Pressure in the Sodium Exposure Test Cell on the Measurements of Electrode Characteristics.....	55
3.2.1.1. Sodium Vapor Pressure Correlation in a Sodium Exposure Test Cell.....	56
3.2.1.2. Thermal FEA Model of a Sodium Exposure Test Cell.....	58
3.2.2. Validation of the Electrode/Electrolyte Geometry in SETC.....	58
3.3. Experimental Procedure.....	62
CHAPTER IV RESULTS AND DISCUSSION.....	67
4.1. Introduction of Results.....	67
4.2. Effect of Sodium Vapor Pressure in SETC.....	68
4.2.1. Evaluation of Sodium Vapor Pressure Correlations.....	69
4.2.2. Evaluation of the Sodium Vapor Source Temperature Distribution in SETC.....	70
4.3. Geometry Effect.....	73
CHAPTER V FINDINGS, CONCLUSION AND RECOMMENDATIONS.....	87
5.1. Summary.....	87
5.2. Findings.....	88
5.3. Conclusion.....	89
5.4. Recommendations.....	89
REFERENCES.....	91
APPENDIX A.....	94
APPENDIX B.....	98
APPENDIX C.....	105
APPENDIX D.....	118
APPENDIX E.....	121
VITA.....	124

LIST OF TABLES

TABLE	Page
1. Important parameters for an AMTEC cell.....	40
2. Selected thermodynamic properties with respect to the specified area for FEA analysis.....	64
3. Parameters measured in SETC for two different electrode/electrolyte configurations. Temperature at the electrode 562 ⁰ C. Temperature in the sodium pool 193 ⁰	80
4. Parameters measured in SETC for two different electrode/electrolyte configurations. Temperature at the electrode 698 ⁰ C. Temperature in the sodium pool 230 ⁰	80
5. Parameters measured in SETC for two different electrode/electrolyte configurations. Temperature at the electrode 811 ⁰ C. Temperature in the sodium pool 271 ⁰	80
6. Parameters measured in SETC for two different electrode/electrolyte configurations. Temperature at the electrode 861 ⁰ C. Temperature in the sodium pool 299 ⁰	81
7. R_{act} values measured in SETC for different electrode pairs on the disk at the temperature of the electrode 861 ⁰ C.....	82
8. j_{lim} values measured in SETC for different electrode pairs on the disk at the temperature of the electrode 861 ⁰ C.....	83

LIST OF FIGURES

FIGURE	Page
1. Schematic of multitube AMTEC cell. (a) Elevation; (b) Top view.....	4
2. Schematic of sodium flow at BASE tube wall.....	5
3. Exploded view of the electrode/electrolyte assembly.....	11
4. Idealized unit cell crystal structure of (a) β -alumina and (b) β'' -alumina.....	24
5. Section through the conduction plane of β -alumina.....	25
6. Section through the conduction slab of β'' -alumina.....	26
7. Sodium exposure test cell (SETC).....	42
8. The electrode test sample.....	43
9. A typical IV curve taken from an electrode test sample run in SETC.....	44
10. A typical EIS plot for an electrode test sample in SETC showing the impedance of the electrode/electrolyte assembly as a function of AC frequency.....	45
11. Variables affecting the rate of an electrode reaction in SETC electrode/electrolyte sample.....	46
12. Function structure of the Sodium Exposure Test Cell (SETC).....	50
13. General view of the Sodium Exposure Test Cell experimental setup.....	53
14. Functional view of Sodium Exposure Test Cell experimental setup.....	54
15. Schematic view showing the difference between an (a) SETC and (b) AMTEC electrode/electrolyte configuration.....	60
16. Schematic view of alternative electrode/electrolyte configuration in SETC.....	61

FIGURE	Page
17. Schematic representation of applied thermal loads on SETC.....	63
18. The flowchart of finite element modeling procedure in SETC.....	64
19. Comparison of different correlations and data for the sodium vapor pressure in the Sodium Exposure Test Cell.....	70
20. Graphical representation of the temperature distribution in a SETC with distance; condition (1).....	72
21. Graphical representation of the temperature distribution in a SETC with distance; condition (2).....	72
22. EIS plot of 3-probe measurements for the tube and disk configuration; Temperature at the electrode 562 ⁰ C. Temperature in the sodium pool 193 ⁰ C.....	74
23. EIS plot of 3-probe measurements for the tube and disk configuration; Temperature at the electrode 698 ⁰ C. Temperature in the sodium pool 230 ⁰ C.....	74
24. EIS plot of 3-probe measurements for the tube and disk configuration; Temperature at the electrode 811 ⁰ C. Temperature in the sodium pool 271 ⁰ C.....	75
25. EIS plot of 3-probe measurements for the tube and disk configuration; Temperature at the electrode 861 ⁰ C. Temperature in the sodium pool 299 ⁰ C.....	75
26. IV curve for the disk configuration between electrodes 1-2.....	76
27. IV curve for the disk configuration between electrodes 1-3.....	77
28. IV curve for the disk configuration between electrodes 1-4.....	77
29. IV curve for the disk configuration between electrodes 2-3.....	78
30. IV curve for the disk configuration between electrodes 2-4.....	78
31. IV curve for the disk configuration between electrodes 3-4.....	79
32. Polynomial trends of <i>B</i> value with respect to the electrode temperature for the tube and disk configuration for electrode 1.....	84

FIGURE	Page
33. Polynomial trends of B value with respect to the electrode temperature for the tube and disk configuration for electrode 2.....	84
34. Polynomial trends of B value with respect to the electrode temperature for the tube and disk configuration for electrode 3.....	85
35. Polynomial trends of B value with respect to the electrode temperature for the tube and disk configuration for electrode 4.....	85
36. Equivalent circuit for a simple electrochemical cell, showing the solution resistance R_{sob} double layer capacitance C_{dl} and charge transfer resistance R_{ct}	96
37. Thermal loading; condition (1).....	111
38. Thermal loading; condition (2).....	111
39. Temperature distribution at the hot end of SETC; condition (1).....	112
40. Temperature distribution in the sodium pool; condition (1).....	112
41. Vector plot of temperature gradients in SETC; condition (1).....	113
42. Graphical representation of the temperature gradients in SETC; condition (1).....	113
43. Representation of the temperature distribution on SETC geometry; condition (1).....	114
44. Representation of the temperature gradients on SETC geometry; condition (1).....	114
45. Temperature distribution in the sodium pool; condition (2).....	115
46. Vector plot of temperature gradients in SETC; condition (2).....	115
47. Graphical representation of the temperature gradients in SETC; condition (2).....	116

FIGURE	Page
48. Representation of the temperature distribution on SETC geometry; condition (2).....	116
49. Representation of the temperature gradients on SETC geometry; condition (2).....	117

CHAPTER I

INTRODUCTION

1.1. Motivation for Research

In this century, the future of endeavors in space will depend largely upon the availability of a reliable, inexpensive and robust source of electrical energy. As spacecraft capabilities expand with more diverse objectives, they will require more power from more efficient power systems. Moreover, the limitations of mass and volume imposed by launch vehicles dictate that the higher power levels be produced by lighter and smaller power systems. Therefore, the technologies that are pursued in space power should point toward higher reliability, higher power density, higher efficiency, lower cost and lower volume. Alkali Metal Thermal to Electrical Conversion (AMTEC) is a thermal-to- electric conversion technology that has the potential to meet all these goals and objectives¹.

Ford Motor Company Scientific Laboratory developed the β^- -alumina ceramics as the electrolyte for NaS batteries. In 1968, Ford researchers recognized that the same principle could be applied to a thermally regenerative electrochemical energy conversion system. Through 1979, Ford supported much of the development on what was then called the Sodium Heat Engine. In the 1980's, the Department of Energy (DOE) supported further work on higher power electrochemical cells and electrode development for terrestrial applications. To varying degrees, several other U.S.² and

This thesis follows the style and format of the *Journal of the Electrochemical Society*.

foreign firms began work on the technology also. Interest in space applications surfaced in this time period, and NASA began to support development as well.³ In 1994, the Air Force initiated AMTEC technology development that could be applied to a solar-heated power system for the earth orbiting spacecraft.⁴ NASA and DOE are currently investigating AMTEC as a candidate high-efficiency converter coupled with radioisotope heat sources to power future planetary spacecraft.⁵

With efficiencies of 20 to 30 % possible, AMTEC offers increased power density compared to thermoelectrics, reducing the mass of the power system and the amount of fuel required, while retaining the reliability of a static energy conversion device. Currently, AMTEC cells have reached efficiencies of about 19 %. With deep space probe missions requiring lower system mass, higher efficiency and long lifetimes, both the power density and lifetime of AMTEC cells must be improved. The electrode/electrolyte assembly is a key component in improving the cell's performance.⁶

1.2. Description of AMTEC Operation

AMTEC is a static and direct energy conversion device that converts thermal energy to electricity. The energy conversion is based on the unique properties of the ceramic β'' -alumina solid electrolyte (BASE), which conducts sodium ions through it, while preventing both electron conduction and neutral sodium transport. Figure 1 shows a typical device, which consists of an evaporator, condenser, BASE tubes, porous electrodes, current collectors, α -alumina braze, metal rings and liquid-return artery (wick). To produce power, thermal energy is transferred to sodium, the working fluid, at

the evaporator. The cell has 7 BASE tubes and a central felt-metal wick for returning the liquid sodium working fluid to the cell evaporator. The BASE tubes are brazed to a stainless steel support plate. The low-pressure side (cathode) and high-pressure side (anode) of the β'' -alumina solid electrolyte are covered with porous electrodes and molybdenum mesh current collectors, and the BASE tubes are electrically connected in series. The series connection of AMTEC cell provides the desired d.c. load voltage for the output bus. The thermal energy input to the cell hot plate is transported by conduction and radiation to the BASE tubes and the evaporator structure. The cell has a circumferential radiation shield to reduce parasitic heat losses to the cell wall, a solid conduction stud between the cell hot end and the BASE tubes support plate, and several solid metallic rings around the evaporator. These rings enhance the conduction path between the BASE tubes support plate and the cell evaporator, increasing the evaporator temperature and the sodium anode pressure in the cell. The conical evaporator provides a larger surface area for evaporating the liquid sodium returning from the condenser. The BASE tubes temperature is kept slightly higher than that of the evaporator to prevent condensation of the working fluid onto the anode side of the BASE tube and electrically shorting the BASE tubes in the cell.

Because the BASE supports the sodium pressure differential between the high vapor pressure plenum and the low-pressure cathode region, the joints between the BASE and the metal support plate must be sealed well. High quality, high purity α -alumina, which is compatible with sodium, is used to insulate the BASE tubes electrically from the stainless steel support plate as shown in Figure 1a.⁷

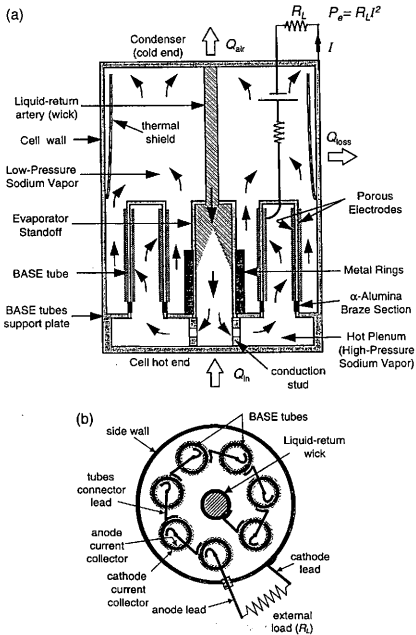


Figure 1. Schematic of multitube AMTEC cell. (a) Elevation; (b) Top view

BASE tube acts as a separator between a high-pressure region containing sodium at about 850°C - 1000°C and low pressure region containing a condenser at 200°C - 400°C .

The high temperature ($\sim 850^{\circ}\text{C}$) sodium vapor is blocked on its way to the condenser by the electrode/electrolyte assembly, creating a high sodium activity gradient across the electrode/electrolyte assembly. Sodium is oxidized at the electrode/electrolyte interface and sodium ions are conducted through the BASE to the low-pressure region of the converter, as shown in Figure 2. Electrons travel through an external load to recombine with sodium ions at a thin, porous electrode, which is deposited onto the outside wall of the BASE tube. The recombined sodium vapor leaves the electrode, collects on the condenser and returns to the sodium reservoir.⁷

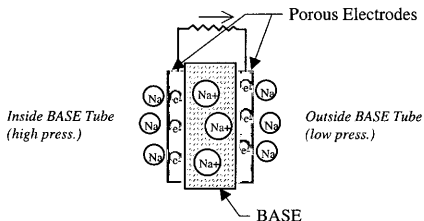


Figure 2. Schematic of sodium flow at BASE tube wall

In order to determine the performance of AMTEC electrodes and compare different electrodes, two parameters are typically used. The morphology factor, G , is the measure of impedance to sodium transport from the electrode/electrolyte interface to the low pressure vapor space,⁸

$$G = \left[\frac{P_{Na}(T_{el}/T_{Na})^{1/2} F}{j_{lim}(2\pi MRT_{el})^{1/2}} - 1 \right] \frac{8\pi}{3} \quad [1]$$

where P_{Na} is the pressure of sodium pool, T_{Na} is the temperature of sodium pool, T_{el} is the temperature of the electrode, M is the molecular weight of sodium, F is a faraday constant and j_{lim} is the limiting current. The normalized exchange current density, B , is the measure of the resistance to the charge transfer at the electrode/electrolyte interface. B is normalized to the sodium collision rate and reaction rate at unit activity of sodium.⁸

$$B = \left[\frac{T_{el}}{P_{el} P_{Na}} \right]^{1/2} \left[\frac{RT_{el}}{R_{act} F} \right] \quad [2]$$

where T_{el} and P_{el} are the electrode temperature and pressure respectively, P_{Na} is the sodium pool pressure, R_{act} is the apparent charge transfer resistance, R is the gas constant and F is the faraday constant. The derivation of B value is given in Appendix E of this work.

One of the experiments used to evaluate the performance of AMTEC electrodes is the Sodium Exposure Test Cell (SETC). Originally designed to perform lifetime studies and materials investigations of AMTEC components including brazes, sodium containment, current collector (typically molybdenum mesh), electrode, and electrolyte, the SETC has become the tool researchers use to quantify and compare electrode performance without the necessity of building an actual AMTEC cell. The utility of the SETC for accurately measuring the parameters previously mentioned is essential to be

able to predict AMTEC electrode performance.⁸ A more in-depth discussion of SETC is given in the apparatus section of this work.

1.3. Objectives of Research and Format of Thesis

The primary goal of this research is to improve the efficiency of AMTEC cell, which is mainly influenced by the performance of its electrodes. The main objective is to determine if the parameters measured within a Sodium Exposure Test Cell (SETC) provide an effective predictor of actual AMTEC electrode performance. The performance of AMTEC electrodes depends on sodium charge exchange and diffusion; which in turn may depend on the electrode/BASE geometry, temperature profile across the electrodes, sodium vapor pressure in the cell, and resistances of electrode/BASE. These can be determined by measuring the values of normalized exchange current density, B , and morphology factor, G , in SETC.

These values can be measured by controlled potential current-voltage curves (iV curves) and Electrochemical Impedance Spectroscopy (EIS) techniques. Current-voltage curves are determined by applying a potential difference between two sample electrodes and measuring the resulting current flow between them. Based on these curves a limiting current can be calculated as well as the series resistance of the cell. EIS is accomplished by applying a small potential, generally 5-10 mV, to the electrode bands and alternating the current initially at high frequency, ~ 65 kHz, reducing it in steps to low frequencies, ~0.1Hz. The resulting impedance is plotted on the complex plane producing an arc with two real axis intercepts. From electrochemical theory, the difference between the high

and low frequency intercepts can be interpreted as the apparent charge transfer resistance of the electrode. The high frequency intercepts value is interpreted as the series resistance of the electrode/electrolyte and connecting leads.⁹

This objective of determining the validity of SETC measurements will be achieved by utilizing different BASE configurations, controlling the sodium vapor pressure within the cell, which is influenced by temperature gradients across the sample, and in the sodium pool, and finally, by identification of errors, which affect the measured parameters of SETC.

The thesis consists of several chapters. The Introduction chapter provides information on the theory of AMTEC cell operation, the electrode/electrolyte assembly's role in the operation, as well as discussion of the parameters currently used as a measure of AMTEC electrode/electrolyte performance. The Literature Review chapter provides information and background about the basic structure, processes, degradation and electrical characteristics of the β'' -alumina solid electrolyte and electrodes used in the experiments. It also provides some information about an AMTEC cell functional requirements and design parameters. The Apparatus and Experimental Procedure chapter describes the methods, experimental procedure, and measurement techniques used to determine the performance characteristics of the AMTEC electrodes. In addition it provides a functional description of a SETC experimental setup. It also discusses the conditions and variables that should be considered in a SETC in order to correctly simulate the processes of an actual AMTEC cell. The Results and Discussion chapter explains the data obtained from the experiments, as well as the adequacy of the

experiment and parameters obtained to evaluate the electrode/electrolyte sample performance. In the Conclusion chapter the results are summarized followed by a list of the important findings. The conclusion that was made is then given. The thesis ends with recommendations for the future research and includes appendix sections at the end for a more detailed discussion of certain subjects related to this research.

CHAPTER II

LITERATURE REVIEW

2.1. Description of the Processes in AMTEC Electrode/Electrolyte Assembly

This chapter describes the basic structure, processes, losses and electrical characteristics of an electrode/electrolyte assembly (BASE tube), the central component of an AMTEC cell. In addition, this chapter gives a more in-depth discussion of the performance characteristics and degradation mechanisms of the electrode/electrolyte assembly at an AMTEC operating environment.

2.1.1. Elements of an Electrode/Electrolyte Assembly

The BASE tube is the basic building block of the AMTEC cell. It has been under intensive development by the Advanced Modular Power Systems (AMPS) and other research institutions.¹⁰ The AMTEC electrode/electrolyte assembly consists of β'' -alumina solid electrolyte (BASE), deposited electrodes, current collector, and leads.

An exploded view of BASE tube assembly is depicted in Figure 3. Electrodes are deposited on inner and outer surface of the BASE. Both electrodes are covered with Mo screens that serve as current collectors to augment the axial electrical conductance. The anode conductance is further augmented by a thick-walled slotted and grooved cylinder, which also serves to press the inner screen against the anode. The cylinder's eight axial slots and circumferential grooves permit passage of sodium vapor to the anode. At the bottom of the slotted cylinder is an eccentric tab that serves as the anode lead, for

connection to the cathode current collector of the next BASE tube in the cell. The bottom of Figure 3 shows a flange that is welded to the BASE tube mounting plate, from which it is electrically isolated by two sapphire insulating rings. The whole assembly is held together and compressively loaded by a metallic load stud. The threaded top end of that stud mates with the assembly's internally threaded top cap.¹⁰

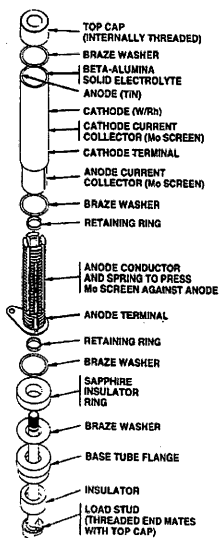


Figure 3. Exploded view of the electrode/electrolyte assembly

2.1.2. Physical Processes in the Electrode/Electrolyte Assembly

Several physical processes occur in an electrode/electrolyte assembly during the electrochemical reaction in an AMTEC cell. These processes include sodium gas diffusion, electrochemical reactions, and ion and electron transfer. The following sections will discuss each of these processes.

2.1.2.1. Sodium Gas Diffusion

Gas diffusion is the mode of transport for the gases in both the porous anode and cathode. At the anode, the mixture of liquid sodium and sodium vapor diffuses into the electrode. Sodium ions diffuse into the cathode and recombined sodium atoms at the electrode/electrolyte interface diffuse out of the cathode. The porosity of thin electrodes used in AMTEC cell varies significantly among the mature films, partly due to the differing surface morphology of the electrodes. The long tube formula for Knudsen flow is inappropriate for modeling the transport properties of the more porous, thin electrodes, since in general the pore length is not much greater than its radius. In this research we use an approximate formula for the pressure drop in cylindrical pores with small l/a ratio.¹¹ The Knudsen flow coefficient can then be explicitly written as

$$K_f = \frac{(2\pi MRT_2)^{1/2}}{F} \left[1 + \frac{l}{\frac{2a}{\pi a^2 N}} \right] \quad [3]$$

where T_2 – the temperature at the anode, M – molecular weight, R – gas constant, F – faraday constant, l – pore length, a – pore diameter, N – number of pores per unit area.

2.1.2.2. Electrochemical Reactions

There are two electrochemical half reactions that occur in the electrode/electrolyte assembly, one at the anode and one at the cathode. The ionization of sodium atoms into sodium ions and electrons occurs at the anode. The theoretical electrochemical equation that represents the anode half reaction is given by equation [4]⁶



In the half reaction at the cathode, sodium ions and electrons recombine to form sodium atoms. The theoretical electrochemical equation that represents the cathode half reaction is given by equation [5]⁶



2.1.2.3. Ion Transfer

The motion of charged defects in an electric field gives rise to an ionic conductivity, which dominates the electrical behavior of an ionic crystal because electronic conductivity is absent. The ions produced at the anode must be transported across the β'' -alumina solid electrolyte to the reaction sites in the cathode. The transport process involves an interaction of ions with each other as well as with oxygen ions in the β'' -alumina ceramics.

The driving force that moves the ions is the positive potential at the anode-BASE interface. This potential results from the buildup of sodium ions at the interface. This force repels the positively charged ions, pushing the outer ions away from the anode.

Ionic conduction in β'' -alumina is anisotropic in nature because it takes place along a plane sandwiched by spinel layers.¹²

2.1.2.4. Electron Transfer

The electrons released by the electrochemical reaction must travel from the anode to the cathode without moving through the β'' -alumina solid electrolyte. Specifically, the electrons travel from a reaction site in the anode, through the gas diffusion region of the anode, the current collector, the external circuit, diffusion region of the adjoining cathode, and finally to a reaction site in the cathode. The process of moving electrons through a material involves electrons colliding with molecules of the material and transferring their energy to the molecules. Each of the excited molecules then releases an electron, which collides with other molecule. A net drift of electrons occurs in the direction of the positive potential, for the electrons the positive potential is the cathode.

2.1.3. Electrical Production

Losses associated with the electrode/electrolyte assembly are called overpotentials or polarization losses, and are separated into activation, ohmic and concentration polarizations. Each type of polarization is influenced by many factors

including the materials used, temperature of BASE, temperature of the condenser, sodium vapor pressure, electrical contacts between electrodes and current collectors, resistance to sodium flow at the interface etc. The following section is a discussion of the maximum theoretical electrode/electrolyte cell potential and each type of overpotential including factors affecting polarization and limiting current in the cell.

2.1.3.1. Theoretical Cell Potential

The Gibbs free energy difference, ΔG , for sodium across the electrolyte is the thermodynamic driving force for sodium ions, and the open circuit voltage, E_{oc} , for such a concentration cell of AMTEC is given as follows

$$\Delta E_{oc} = -\frac{\Delta G}{F} = -\frac{\Delta(H - TS)}{F} = \frac{-v\Delta p + S\Delta T}{F} \quad [6]$$

where F is the Faraday constant, H - the enthalpy, T - the temperature, S - entropy, v - the specific volume, and p - pressure. When the electrolyte for the AMTEC cell is kept at the temperature of the high-temperature side, T_2 , equation [6] can be rewritten as follows, assuming that sodium vapor is an ideal gas:

$$\Delta E_{oc} = -\frac{v\Delta p}{F} = -\left(\frac{RT_2}{F}\right)\left(\frac{\Delta p}{p}\right) \quad [7]$$

where R is the gas constant. Integration of equation [7] from p_h of the high-pressure side to an intermediate pressure, p_m , gives:¹³

$$E_{oc} = \left(\frac{RT_2}{F} \right) \ln \left(\frac{p_h}{p_m} \right) \quad [8]$$

At open circuit, Na^+ ions are driven by thermal kinetic energy toward the low-pressure BASE surface, causing this surface to acquire a net positive charge. The electric field in the BASE builds up until it is strong enough to stop the flow of Na^+ . The open circuit voltage E_{oc} is dependent upon the activity (vapor pressure) of sodium at the high temperature and the vapor pressure of sodium at the electrode-BASE interface, p_m , which is in equilibrium with sodium at the condenser, p_1 , according to the Nernst equation. The dependence of p_m on p_1 at zero current density is given by equation.¹

$$p_m(i=0) = p_1 \left(\frac{T_2}{T_1} \right)^{\frac{1}{2}} \quad [9]$$

When the external circuit is closed, electrons flow through the load, neutralizing sodium ions at the BASE/porous electrode interface. Sodium atoms absorb their heat of vaporization, leave the porous electrode, move through the vapor space, and release their heat of condensation on the condenser surface at T_1 . The voltage developed across the BASE separator forces electrons to flow to the porous electrode through the load, producing electrical work.¹

Originally, current voltage models were based on Weber's first 1974 formulation.¹⁴

$$E = A - B \log i - iR_0 \quad [10]$$

where E is the voltage at steady state, i is the current at steady state, R_0 is the surface electrical resistivity of the solid electrolyte.

This formulation did not take into account two important loss mechanisms associated with real electrode effects: charge exchange kinetics and transport losses. The early model was found to compare reasonably well with the best high power molybdenum electrode data. However, the performance of those electrodes was found to be transient in nature due to the presence of inadvertently formed *Na-Mo-O* compounds that enhance both sodium transport through the electrode and interfacial kinetics. These compounds decompose and evaporate under typical AMTEC operating conditions, and the resulting performance cannot be modeled accurately without including the resultant larger kinetics and transport losses.¹

As a result, a new detailed model that includes the previously neglected phenomena has been developed at JPL and a new current versus voltage expression for AMTEC has been derived. The new expression is based on the electrochemical current overpotential equation.

Current density is given in A/cm^2 , by:

$$i = i_0 \left(\exp[-\alpha\eta f] - \left[\frac{(p_j + \Delta p + p_4)}{p_4} \right] \exp[(1-\alpha)\eta f] \right) \quad [11]$$

The cell voltage, V is contained in the definition of:

$$\eta = V - E_{oc} + iR_{tot} \quad [12]$$

R_{tot} is the total ohmic resistance of the cell and E_{oc} is the open circuit voltage. p_j is the pressure due to sodium leaving the electrode, Δp is the sodium vapor pressure drop

within the pore, and p_4 is the sodium pressure at the electrode when no current flows due to evaporation at the condenser,

$$f = \frac{F}{RT_2} \quad [13]$$

where F is Faraday's constant, and R is the gas constant, i_0 is the exchange current density and α is the electrochemical transfer coefficient. Δp is a function of pore geometry that is expressed by a dimensionless morphology factor, G .¹

2.1.3.2. Overpotential

When an electrolytic cell is under equilibrium conditions no current passes through the cell, and both electrodes are at their equilibrium potentials; the algebraic sum of these gives E^0 , the theoretical e.m.f. of the cell reaction. For the system to be displaced from equilibrium, an e.m.f. greater than E^0 must be applied. Electrolysis will then begin, and the current flowing through the cell will indicate the rate of the chemical reaction-taking place. This phenomenon can be described by the Nernst equation:¹⁵

$$E(R, O) = E^0(R, O) + \frac{RT}{nF} \ln \frac{a(\text{oxidised state})}{a(\text{reduced state})} \quad [14]$$

where E^0 is the potential at normal conditions (pressure is 1atm, temperature is 25°C), T is the temperature, F is Faraday's constant, R is the gas constant, n is the number of electrons, a is the activity of species.

One way in which the energy supplied by the external source is expended is in overcoming the resistance of the solution to the passage of the current. But after

allowing for this voltage drop through the solution, there still remains an amount by which the applied e.m.f. exceeds E_{eq} . This difference is the overpotential, η .

$$\eta = E - E_{eq} \quad [15]$$

where E is the applied e.m.f. and E_{eq} is the e.m.f. at the equilibrium state.

Since it must be concerned with conditions at the two electrodes, it is best to study this separately. The extent by which the cathode potential is found to be more negative than its equilibrium value is the cathode overpotential, and, similarly, a working anode will be more positive than its equilibrium value by an amount corresponding to the anode overpotential.¹⁵

At least two, and sometimes three, causes of overpotential can be distinguished. In the first place, the passage of current immediately alters the concentration of the reactive ion at the electrode surface, and the potential needed to maintain current flow will increase. This change is called concentration overpotential. A second type of overpotential is activation overpotential. The relative importance of this second overpotential varies greatly; for a process that takes place readily it will be small, but it can be large for an electrode process that requires high activation energy. The third cause of overpotential is present when an electrode is covered by an adherent surface layer of poorly conducting material. The resistance may be so high that a very large potential drop through this surface film is included in the overpotential measurement.

The overpotential at an electrode (for a given current density) is the sum of these effects: the concentration, activation and film resistance (ohmic) overpotentials

$$\eta = \eta_{conc} + \eta_{act} + \eta_{ohm} \quad [16]$$

The third is really a spurious effect, which is easily recognized, if present. Of the other two, the first is concerned with the solution side of the interface, the second with the electron transfer over the interface.

The following is a detail explanation of each overpotential type.

Activation Overpotential

Activation overpotential is present when the rate of an electrochemical reaction at an electrode surface is controlled by sluggish electrode kinetics. In other words, activation overpotential is directly related to the rates of electrochemical reactions. There is a close similarity between electrochemical and chemical reactions in that both involve an activation barrier that must be overcome by the species. Activation overpotential is described by the general form of the Tafel equation¹⁵

$$\eta_{act} = \frac{RT}{\alpha nF} \ln \frac{i}{i_0} \quad [17]$$

where α is the electron transfer coefficient of the reaction at the electrode being addressed, and i_0 is the exchange current density.

Ohmic Overpotential

Ohmic losses occur because of resistance to the flow of ions in the electrolyte and resistance to the flow of electrons through the electrode materials. The dominant ohmic losses, through the electrolyte, are reduced by decreasing the electrode separation

and enhancing the ionic conductivity of the electrolyte. Because both the electrolyte and electrodes obey Ohm's law, the ohmic losses can be expressed by the equation¹⁵

$$\eta_{ohm} = iR_{tot} \quad [18]$$

where i is the current flowing through the cell, and R_{tot} is the total cell resistance, which includes electronic, ionic, and contact resistance.

Concentration Overpotential

As a reactant is consumed at the electrode by electrochemical reaction, there is a loss of potential due to the inability of the surrounding material to maintain the initial concentration of the bulk fluid. That is, a concentration gradient is formed. Several processes may contribute to concentration overpotential: slow diffusion in the gas phase in the electrode pores, solution/dissolution of reactants/products into/out of the electrolyte, or diffusion of reactants/products through the electrolyte to/from the electrochemical reaction site. At practical current densities, slow transport of reactants/products to/from the electrochemical reaction site is a major contributor to concentration overpotential¹⁵

$$\eta_{conc} = \frac{RT}{nF} \ln \left(1 - \frac{i}{i_L} \right) \quad [19]$$

where i_L is the limiting current.

2.1.3.3. Limiting Current

The rate of mass transport to an electrode surface in many cases can be described by Fick's first law of diffusion

$$i = \frac{nFD(C_B - C_S)}{\delta} \quad [20]$$

where D is the diffusion coefficient of the reacting species, C_B is its bulk concentration, C_S is its surface concentration, and δ is the thickness of the diffusion layer. The limiting current i_L is a measure of the maximum rate at which a reactant can be supplied to an electrode, and occurs when $C_S = 0$, i.e.,¹⁶

$$i_L = \frac{nFDC_B}{\delta} \quad [21]$$

2.2. β'' -alumina Solid Electrolyte

β'' -alumina is a classic example of a class of material known as superionic conductors, so called because they are capable of carrying an electric current while still in the ionic crystal. In β'' -alumina, sodium ions, which are confined to specific conduction planes within the ionic crystal, are highly mobile and thus readily carry an electric current when an electric field is applied. This section gives some insights about the structure, composition and ionic conductivity mechanisms of β'' -alumina solid electrolytes. In addition, this section discusses the differences between β -alumina and β'' -alumina solid electrolytes.

2.2.1. Overview of β' -alumina Group Ceramics

β' -alumina was first reported as long ago as 1916 but initially it was not appreciated that sodium is an essential constituent of the material. That β' -alumina is actually a sodium aluminum oxide was established during the first crystal structure analysis when the formula of β' -alumina was established as $Na_2O \cdot 11Al_2O_3$. It has since become clear that β' -alumina is never stoichiometric as prepared and the formula $(Na_2O)_{1+x} \cdot 11Al_2O_3$ is more appropriate, but the original name remains in general use.¹⁷

2.2.2. Structure of β -alumina Group Oxides

The β -alumina group of oxides is characterized by structures composed of alternating slabs of close packed oxide and layers with a low atom density containing mobile sodium cations.¹⁴ Most of the information concerning the structure of β' -alumina has been obtained using x-ray diffraction, although in recent years several other experimental probes have been applied to determine details of the structure and conductivity mechanism. The basic crystal of β' -alumina was established by Beevers and Ross in 1937.¹⁷ The structure they determined is shown in the Figure 4. The blocks of Al^{3+} and O^{2-} are packed in the same fashion as the packing in spinel, $MgAl_2O_4$, and are usually called "spinel blocks". In this case, Al^{3+} ions occupy the octahedral sites as well as the tetrahedral sites occupied by Mg^{2+} ions in spinel. The spinel - type blocks are separated by a loosely packed plane containing Na^+ and O^{2-} . Because of the loose packing, space is available for movement of the sodium ions leading to the high ionic conductivity shown by β -alumina. However, conductivity is limited to this plane and

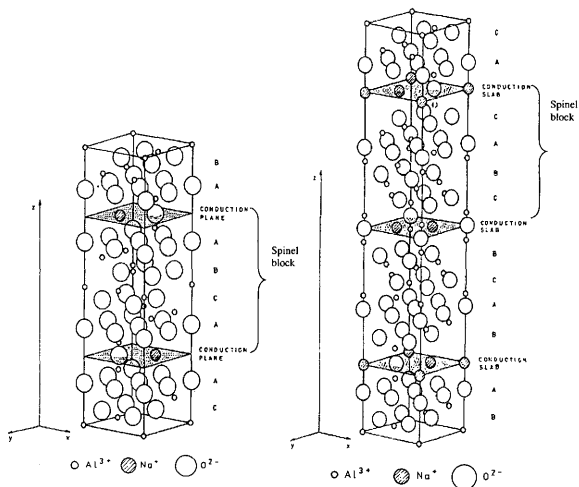


Figure 4. Idealized unit cell crystal structure of (a) β -alumina and (b) β' -alumina

movement along the z -axis is exceedingly difficult. The material, therefore, is highly anisotropic.¹⁸ There are two main subgroups that differ in the stacking sequence of layers up the unique axis. The first group (β) is stacked according to a twofold screw axis, contains a mirror plane through the layers of mobile cations and results in hexagonal crystal structures. The idealized structure of the unit cell of β -alumina is

shown in Figure 4 (a). Figure 5 shows the conducting plane of β -alumina. Ionic diffusion occurs exclusively within this conducting plane perpendicular to the z-axis.

The second subgroup (β'') is stacked according to a threefold screw axis, contains no mirror plane and has rhombohedral structures. The idealized structure of β'' -alumina is shown in Figure 4 (b). The unit cell is 50 % larger than that of β -alumina by virtue of the difference in stacking sequence. Adjacent close packed oxide slabs are held apart by $Al - O - Al$ spacer units, but in this structure alternate sodium atom sites lie above and below the plane through the center of the oxide spacer atoms and the Na^+ ion diffusion path actually encompasses a finite volume (the conduction slab) rather than a plane as in the beta alumina structure as shown in Figure 6.¹⁸

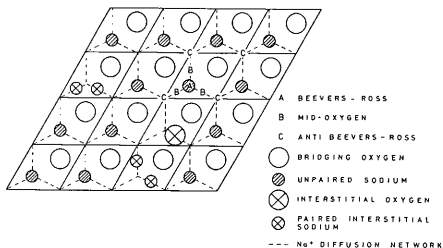


Figure 5. Section through the conduction plane of β -alumina

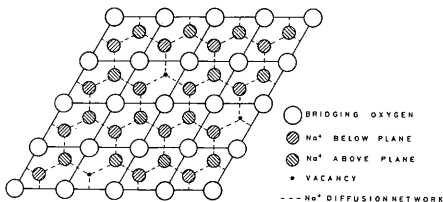


Figure 6. Section through the conduction slab of β' -alumina

2.2.3. Ionic Conductivity and Diffusion Mechanisms in β' -alumina

In nearly perfect crystals, atomic (ionic) diffusion is always connected to the existence of lattice defects.¹⁶ The most common types of diffusion in crystals are diffusion through vacancies (vacancy diffusion) and diffusion in through interstitial sites (interstitial diffusion). In ionic crystals such as β' -alumina such motion of ions under the influence of an external field creates a net ionic current. The ionic conductivity is generally described by an Arrhenius equation¹⁹

$$\sigma = \left(\frac{C}{kT} \right) \exp\left(\frac{-u}{kT} \right) \quad [22]$$

where u is the activation energy of ion motion, C the pre-exponential factor, k the Boltzmann constant, and T the temperature. C is given by

$$C = \left(\frac{1}{3}\right)(Ze)^2 n \lambda^2 \nu \quad [23]$$

where Ze is the charge of the conducting ion, n is the density of defects (the density of vacancies in vacancy diffusion or the density of interstitial ions in interstitial diffusion), λ is the unit jump distance of the ion, usually the closest ionic pair distance, and ν is the jump frequency.¹⁹ The corresponding diffusion coefficient D is defined by

$$D = D_0 \exp\left(\frac{-u}{kT}\right) \quad [24]$$

where

$$D_0 = \frac{C}{(Z^2 e^2 n)} \quad [25]$$

and hence

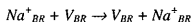
$$\sigma = n(Ze)^2 \frac{D}{(kT)} \quad [26]$$

The β' -alumina type of crystal structure is ideally equipped for good ionic transport in the conduction planes, having a high proportion of defect sites for the mobile

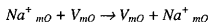
ions linked by networks of easy access.¹⁸ One of the properties of β'' -alumina is the ability to replace sodium ions by other metal cations using ion exchange techniques.¹⁹

In β'' - alumina Beever Ross (BR) and anti Beever Ross (aBR) sites are identical and represent one set of sites which would be completely filled for stoichiometric $Na_2MgAl_{10}O_{17}$. However, this material is sodium deficient, and vacancies in this set of sites will be present. If BR sites are considered as lattice sites while aBR or MO (midoxygen) sites are interstitial sites there are three conduction mechanisms that can be postulated for β'' -alumina:

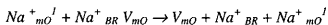
- 1) Vacancy



- 2) Interstitial (direct interstitial movement)



- 3) Interstitialcy (indirect interstitial movement)



One experimental method to help decide which of these mechanisms is responsible for conductivity is to compare tracer diffusion coefficients D_t with diffusion coefficient calculated from conductivity measurements D_σ using the Nernst-Einstein equation¹⁹

$$D_\sigma = \frac{\sigma RT}{cq^2} \quad [27]$$

where c is the concentration of mobile ions and q is their charge. The two diffusion coefficients differ because of different jump distances between tracer movement and

charge movement and the correlation factor, f . The diffusion coefficients can be given by the following equations¹⁶

$$D_i = \Gamma \lambda_i^2 \nu_i f \quad [28]$$

$$D_\sigma = \Gamma \lambda_\sigma^2 \nu_\sigma \quad [29]$$

(where Γ is a geometric factor = 1/6 for cubic three – dimensional motion, λ is jump distance, and ν is jump frequency)

$$\frac{D_i}{D_\sigma} = \left(\frac{\lambda_i}{\lambda_\sigma} \right)^2 \frac{\nu_i}{\nu_\sigma} f = H_R \quad (\text{Haven ratio}) \quad [30]$$

The factor f is introduced for tracer jumps because they may not be completely random, e.g., there will be a correlation between successive steps of a particle moving by a vacancy mechanism even if the steps of the vacancies themselves are uncorrelated. Thus, D_i contains a correlation factor while D_σ does not. However, it should be noted that these relationships have been developed for defect models, which contain a small concentration of defects.

In general, it is usually assumed that $\nu_\sigma = \nu_i$ and then a measurement of H_R can be used to help elucidate the conduction mechanism. For the vacancy mechanism $\lambda_i = \lambda_\sigma$ and $f \cong 0.3 - 0.8$ depending on geometrical configuration. Direct interstitial jumps are not correlated ($f = 1$) and $\lambda_i = \lambda_\sigma$ so that $H_R = 1$. On the other hand when the conduction mechanism is indirect, $\lambda_i < \lambda_\sigma$ and $f \neq 1$ and $H_R \neq f$.¹⁹

2.2.4. Composition and Phase Relationships of β'' -alumina

The β -alumina structures are remarkable not only for their ionic conductivities but also for their versatilities for isomorphous replacement.¹⁷ The stoichiometry of β'' -alumina has long been the subject of some speculation. Traditionally, the stoichiometries of both β and β'' alumina are referred back to the so called ideal 1:11 stoichiometry of Beevers and Ross, with formula $NaAl_{11}O_{17}$, although real materials contain more soda than given in this formula.¹⁸

Several types of phase diagrams have been proposed successfully. For an amount of alumina greater than 50 mol % two stable phases appear in the $Na_2O - Al_2O_3$ system:

- (1) The $NaAlO_2$ aluminate in three allotropic forms: β , γ , δ
- (2) The β alumina, a non stoichiometric phase of composition between $5.3 Al_2O_3$, Na_2O and $8.5 Al_2O_3$, Na_2O . Its domain increases from 1050 to 1400°C and then decreases on the side rich in sodium oxide. The domain disappears around 2000°C at a peritectic point where the composition is about $8.5 Al_2O_3$, Na_2O . The ideal composition, considered for a long time as $11 Al_2O_3$, Na_2O is never reached. The two phases are separated by an eutectic at 1580°C.¹⁷

During preparation of β -alumina, a metastable form, β'' -alumina, is often encountered. Discovered with large amounts of sodium oxide, it is also a nonstoichiometric phase of composition between 5.33 and $8.5 Al_2O_3$, Na_2O . At 1550°C β'' -alumina is transformed irreversibly into β -alumina. β'' alumina is always

accompanied by β from the moment of its formation. In the β and β'' aluminas domain of coexistence for the same temperature and the same heat treatment the proportions of β (stable) to β'' (metastable) practically do not vary as the amount of Al_2O_3 varies. β'' -alumina, however, can be stabilized by the introduction of impurities.²⁰

2.3. Performance Characteristics of AMTEC Electrode/Electrolyte Assembly Components

An AMTEC cell has been considered an attractive power source for a variety of long-term space missions as well as terrestrial applications. Durability requirements and high temperature operation of AMTEC have driven the need to investigate potential performance degradation of β'' -alumina solid electrolyte and electrodes. The following sections give some insights about characteristics and degradation phenomena of β'' -alumina solid electrolyte and porous electrodes at AMTEC operating conditions.

2.3.1. Performance Degradation of β'' -alumina Solid Electrolyte at AMTEC Operating Conditions

Alkali oxide loss from β'' -alumina solid electrolyte at AMTEC operating conditions is a concern related to evaporation rate of sodium oxides to low pressure sodium vapor at temperatures of 900-1200^oC. If sodium oxide loss continues

indefinitely, the β'' -alumina solid electrolyte (BASE) ceramic would eventually be destroyed.¹⁸

There is an interest in the thermal decomposition of BASE at $900\text{ }^{\circ}\text{C} < T < 1200\text{ }^{\circ}\text{C}$ in vacuum and at low sodium gas pressures, in interactions of BASE with liquid sodium or high pressure sodium gas, and also in decomposition induced by reaction with metal vapor or other contaminants under given conditions. It is critically important to the β'' -alumina solid electrolyte not suffer a major loss of ionic conductivity near its surface. It would be tolerable if some of the β'' -alumina phase were converted to the β phase near the surface, since the beta phase is still a good ionic conductor, but device failure would occur if there were conversion of β'' -alumina to α -alumina through loss of all sodium oxide at the surface. Both failure due to α -alumina formation and the performance degradation due to moderate conductivity decrease must be incorporated into the AMTEC life model.²¹

Sodium β' -alumina is one of the best-characterized solid electrolytes, but its high temperature chemistry in the range of $500\text{ }^{\circ}\text{C}$ to $1500\text{ }^{\circ}\text{C}$ is only partly understood. In particular, the kinetics of slow degradation reaction of sodium β' -alumina have not been definitely characterized. Experiments show that there is sodium oxide loss from β' -alumina. This sodium oxide loss is strongly thermally activated and strongly suppressed by sodium gas pressure.²²

The investigation of high temperature processes in the range $900\text{ }^{\circ}\text{C}$ to $1200\text{ }^{\circ}\text{C}$ which may lead to degradation of sodium β' -alumina in AMTEC devices has been done by JPL (Jet Propulsion Laboratory). Modeling done at JPL predicted very slow and

highly activated loss of sodium oxide into a gas phase comprised of low to moderate pressure sodium gas and extremely low pressure oxygen at typical AMTEC operating conditions. Experiments have provided some conformation for this prediction. Sodium oxide loss is strongly thermally activated and strongly suppressed by sodium gas pressure. Faster thermal degradation by several evaporated transition metals on β'' -alumina yielding sodium gas is thermodynamically possible. Experiments showed that chromium and manganese lead to formation of Cr_2O_3/Al_3O_3 and $MnAl_2O_4$ after hundreds of hours at 900 °C to 1200 °C, but reaction with iron is much slower or negligible under these conditions.²¹

Phase change is the most important part describing the degradation of β'' -alumina, which has three main functions: BASE weight loss, sodium loss, and reactions between β'' -alumina and components. Experiments indicate that sodium oxide loss from β'' -alumina into low oxygen activity liquid sodium does not occur at a significant rate at 900 °C. Under the some conditions, decomposition of 99,8% α -alumina to form $NaAlO_2$ is fairly rapid. It is evident that both sodium β -alumina and sodium β'' -alumina are thermodynamically stable phases at appropriate activities of sodium and oxygen.²³ Some uncertainty in the values of the free energies of formation of these phases remains, as does a quantitative understanding of the effect of spinel block stabilizing ions on the thermodynamic stability of the β'' and β phases. The β'' -alumina phase is stabilized by spinel block stabilizing ions such as Li^+ and Mg^{2+} .²² These stabilizing ions do confer greater stability, and seem to be necessary for the high temperature processing which

yields pure, dense BASE ceramics.²⁰ Phase studies indicate that pure sodium β'' - alumina is not formed without stabilizing ions.¹⁷

2.3.2. Performance Characterization of AMTEC Electrodes

Tests done in AMTEC research have shown that, the electrode is the component most likely to influence device performance and limit operating lifetime. In order to select an ideal AMTEC electrode it is required to know characteristics of an electrode its degradation mechanisms and also the environment to which that particular electrode will be exposed. In addition, it is important to determine the relationship between electrode performance and operating and design parameters of the entire cell.

2.3.2.1. AMTEC Electrode Requirements

An AMTEC electrode must meet the following requirements in order to achieve the desired performance.

- The electrodes must be stable for long periods of time at AMTEC operating temperatures (700-1000⁰C).
- The electrode must be chemically and thermally compatible with other components in the cell, including sodium and the β'' -alumina solid electrolyte. It must not form new phases with other components of the cell, which would adversely affect the performance of the cell.
- The electrode must provide reaction sites for sodium reduction and oxidation to occur.

- The electrode must provide a path for electrons from the sodium oxidation sites to the current collector, and from the current collector to the sodium reduction sites.
- The electrode must provide a means of sodium transport between the reaction sites and the vapor space.

2.3.2.2. AMTEC Electrode Characteristics

In order to find materials meeting the requirements stated above, certain characteristics and properties of both metals and ceramics should be investigated, which should help focus the search for an advanced electrode. To address the stability requirements, metal and ceramic electrodes should have melting points substantially above AMTEC operating temperatures. A high melting temperature generally corresponds to a low vapor pressure and a low surface diffusion coefficient, which both contribute to the chemical and morphological stability of the electrode.⁶

Low vapor pressure reduces the chance of contaminating other components in the cell and helps ensure that a sufficient amount of electrode remains after an extended time at high temperature. A low surface self-diffusion coefficient corresponds to a slow sintering behavior, helping to maintain a stable physical morphology over the lifetime of the electrode. Sintering behavior is particularly important in AMTEC electrodes, since the reaction sites occur only at the three-phase boundary between electrode, electrolyte, and sodium vapor space in electrode without internal sodium transport modes.²

The coefficient of thermal expansion must also be taken into account when selecting an electrode; although, very thin, hence not subject to great internal stresses,

the electrode must remain bonded to the electrolyte. Porous metal electrodes should have a greater tolerance to differences between electrode and electrolyte thermal expansion, compared to the ceramics. Electrode material candidates with higher surface self-diffusion coefficients or thermal expansion coefficients that don't match the electrolyte might be used in a cermet electrode with β'' -alumina. Cermet electrodes offer the potential to increase reaction site density per unit electrode surface area and maintain the porosity of the electrode by forming a framework of β'' -alumina to help control the sintering behavior of the metal. The cermet can also effectively adjust the coefficient of thermal expansion of the electrode to help reduce thermal stresses.

Other necessary characteristics include having no reaction with sodium and the β'' -alumina electrolyte. A ceramic electrode should have a sufficiently negative Gibbs free energy at AMTEC operating temperatures to keep material losses due to dissociation small enough that they don't interfere with cell operation.

Once compatibility is addressed, the electrical resistance and sodium transport mechanisms must be examined. Although electrical resistance and sodium conduction are both properties of the material, the physical morphology of the electrode plays an equally important part. Characteristics of the electrode, such as the porosity, thickness, grain size, and quality of contact at the electrode-electrolyte interface, can all affect the condition of both electrons and sodium to and from the reaction sites.

The porosity of the electrode affects both sodium transport and electrical conductivity. Increasing porosity increases an electrode's sodium transport capability,

while reducing its electrical conductivity; therefore, an optimized porosity must be achieved. Porosity plays important role in identifying the mode of sodium transport.²⁴

2.3.2.3. Sodium Transport Modes in AMTEC Electrodes

Transport of alkali metal atom through porous electrode of AMTEC cell is responsible for significant, reducible losses in the electrical performance of these cells. Sodium transport has been characterized in a variety of AMTEC electrodes and several different transport modes clearly exist.

Transport mechanisms include free molecular flow, surface and grain boundary diffusion of sodium, bulk diffusion of sodium atoms through condensed phases, and sodium ion conduction with charge transfer at the electrode exterior surface.

Free molecular flow is the dominant transport mechanism in clean porous molybdenum and tungsten electrodes, and contributes to sodium transport in all porous electrodes, including WPt_2 , WRh_3 and TiN .²⁵ Using a free-molecular flow model, the value of morphology factor, G , for these electrodes can be determined from impedance data.

Molybdenum and tungsten electrodes containing phases such as Na_2MoO_4 and Na_2WO_4 exhibit very efficient sodium ion transport through the electrode in the ionic conducting phase.²⁶ These electrodes also show reversible electrochemical reaction in which sodium ions and electrons are inserted into or removed from phases such as Na_2MoO_4 and $Na_2Mo_3O_6$, which are present in the electrode.

WPt_2 and WRh_3 electrodes typically exhibit both free molecular flow transport as well as an enhanced thermally activated transport mode, which is probably surface and grain boundary diffusion of sodium in the alloy electrode.²⁷ Sodium transport away from these electrodes is affected by both the electrode's properties and the exterior environment that inhibits sodium gas flow to the condenser.

Titanium nitride, TiN , electrodes used in AMTEC cells, and similar electronically conducting refractory compounds such as TiB_2 and NbN are always physically porous to some degree as formed by sputter deposition or screen printing, and those compounds sinter quite slowly. Hence free molecular flow is always a significant sodium transport mode in these electrodes. Some TiN electrodes also have been found to exhibit electrochemical reactions involving electrode phases, which persist in sodium exposure test cell at 950 °C.²⁵

2.3.2.4. Performance Optimization of AMTEC Electrodes

In order to optimize performance of AMTEC electrodes it is crucial to identify all losses and minimize internal resistances within the cell. The losses include pressure loss due to sodium flow through the device, heat loss within the cell and resistances including contact and sheet resistances, and apparent charge transfer resistance, R_{act} , which is potential-dependant resistance. The impedance to sodium flow and charge transfer must be minimized and optimum values of normalized exchange current density, B , and morphology factor, G , should be obtained.

In order to effectively identify all losses in AMTEC electrodes and model optimum performance characteristics the following issues should be addressed:

1. Determination of all functions the system must fulfill.
2. Determination of all functional requirements.
3. Determination of all critical parameters and constrains in the system.
4. Determination of the relationship between functions and parameters.
5. Determination of errors in the system.

Many parameters are associated with AMTEC power systems; parameters are anything that affects the design or performance of the system. An abbreviated list of the parameters of AMTEC cell is shown in Table 1. The list is separated into operating and design parameters. Operating parameters deal with the AMTEC cell operating conditions whereas the design parameters are those associated with the system configuration.

To understand the relative importance of the parameters and parameter interactions an investigation of the parameters are needed.

Table 1. Important parameters for an AMTEC cell

Parameter	Description
Operating	
<ul style="list-style-type: none"> Sodium vapor pressure at the cathode 	Pressure of the low activity sodium at the cathode
<ul style="list-style-type: none"> Sodium vapor pressure drop within the pore 	Pressure difference within the cathode, from electrode/electrolyte interface to outer surface of cathode
<ul style="list-style-type: none"> Temperature of the evaporator 	Temperature of sodium at the evaporator, about 900-1000 K: high activity sodium
<ul style="list-style-type: none"> Temperature at the condenser 	Temperature of the condenser, about 400-700 K
Design	
Electrode/Electrolyte Assembly	
<ul style="list-style-type: none"> BASE 	Type and thickness of the material and configuration. Material of BASE is β "alumina solid electrolyte ($\text{Na}_{5/3}\text{Li}_{1/3}\text{Al}_{32/3}\text{O}_{17}$).
<ul style="list-style-type: none"> Electrode 	Material of the electrode, morphology and physical bond with the BASE .
<ul style="list-style-type: none"> Current collector 	Type, material and configuration of the current collector.
<ul style="list-style-type: none"> α-alumina braze 	Material and configuration of α -alumina braze.
Cell Assembly	
<ul style="list-style-type: none"> Sodium return artery 	Wick structure, pressure drop in the return artery, effective capillary maximum pore radius of the wick.
<ul style="list-style-type: none"> Thermal shield 	Material, configuration and emissivity of condenser wall.
<ul style="list-style-type: none"> Evaporator 	Material, configuration and thermal conductivity of the evaporator.
<ul style="list-style-type: none"> Condenser 	The condenser configuration and material.

CHAPTER III

APPARATUS AND EXPERIMENTAL PROCEDURE

This chapter describes the methods and techniques used in order to meet the objectives stated previously and to determine the processes and electrical characteristics of AMTEC electrodes. Complete explanation of the experimental setup is given by discussing the procedure and materials used in the experiments. In addition, the difference between an AMTEC and a SETC electrode/electrolyte configuration is described.

3.1. Apparatus

In order to accurately evaluate the performance of AMTEC electrodes it is important to provide appropriate operational conditions. These conditions can be simulated using appropriate devices and instruments, and the performance characteristics of AMTEC electrodes can be obtained. The following sections describe the experimental apparatus and procedure used in this research.

3.1.1. The Sodium Exposure Test Cell

In order to isolate components and determine degrees of interaction we use the Sodium Exposure Test Cell (SETC). SETC plays an important role in accelerating testing to develop life models for various components of an actual AMTEC cell, to

determine the models of interaction among components, and finally to verify life models.⁸

The Sodium Exposure Test Cell is non-power producing cell used to evaluate the performance of AMTEC electrodes. As shown in Figure 7, the SETC consists of a stainless steel tube chamber evacuated and then heated at one end to AMTEC operating temperatures and kept at condenser temperatures near the sodium containment. At the containment sodium pool provides a vapor pressure of the same order of magnitude as that found on the low-pressure side of AMTEC cells. The chamber is lined with a refractory metal to remain consistent with actual AMTEC cell and prevent volatiles from the stainless steel such as chromium and manganese from reacting with the test samples.

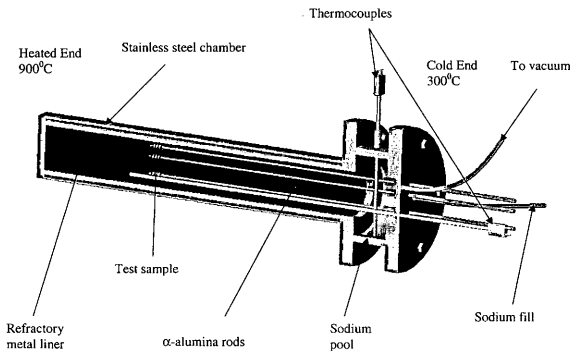


Figure 7. Sodium exposure test cell (SETC)

The 4 test samples which are placed near the hot end, consist of a cylindrical β'' -alumina electrolyte, see Figure 8, with 4 electrode bands approximately 0.25 cm wide deposited on the outer surface separated by 0.25cm spaces. Leads are attached to each electrode and threaded through electrically insulated feedthroughs at the manifold. Thermocouples are placed at the hot space near the electrodes and in the sodium pool.

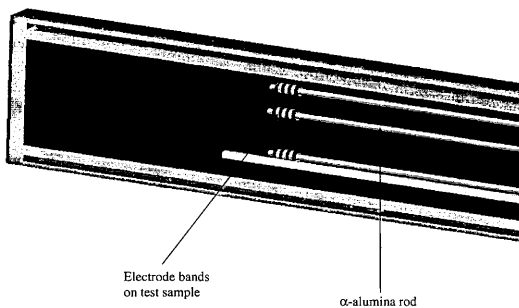


Figure 8. The electrode test sample

Two types of measurements are made on SETC sample, controlled potential current-voltage curves (iV curves) and Electrochemical Impedance Spectroscopy (EIS). Current-voltage curves, see Figure 9, are measured by applying a potential difference between

two electrode bands and measuring the resulting current flow between them. Based on these curves a limiting current can be calculated as well as the series resistance of the cell. EIS is accomplished by applying a small potential, generally 5-10 mV, to the electrode bands and alternating the current initially at high frequency, ~ 65 kHz, reducing it in steps to low frequencies, ~0.1Hz. The resulting impedance is plotted on the complex plane producing an arc with two real axis intercepts as shown in Figure 10. From electrochemical theory, the difference between the high and low frequency intercepts can be interpreted as the apparent charge transfer resistance of the electrode. The high frequency intercepts value is interpreted as the series resistance of the electrode and connecting leads.

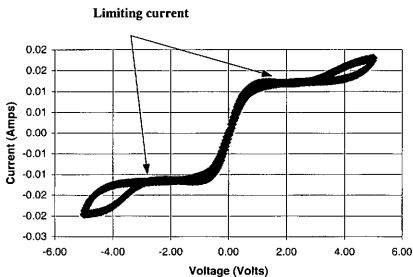


Figure 9. A typical IV curve taken from an electrode test sample run in an SETC

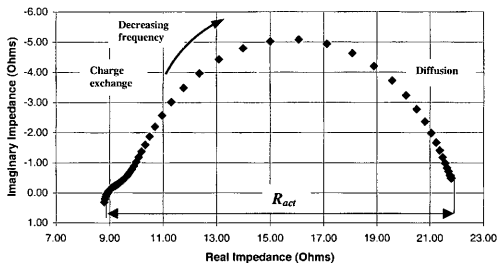


Figure 10. A typical EIS plot for an electrode test sample in an SETC showing the impedance of the electrode/electrolyte assembly as a function of AC frequency

3.1.1.1. Performance Optimization of a Sodium Exposure Test Cell

In order to obtain accurate results and correlate data obtained from SETC model with data from AMTEC model it is very important to go through identification and resolving of inconsistencies in the measurements of performance data. Only considering all these inconsistencies it will be possible to effectively quantify the relationship between design parameters, operational parameters and AMTEC performance, and hence develop efficient AMTEC model.

Variables in SETC Specimen

An investigation of the electrochemical behavior of a system consists of holding certain variables of the electrochemical cell constant and observing how other variables

vary with changes in the controlled variables. Figure 11 represents a test specimen with 2 pairs of electrodes. This specimen is placed in the high temperature SETC chamber. The parameters of importance in the electrochemical cell are shown in Figure 11. Since no current flows when $i = 0$, and E is determined as a function of concentration, no net faradaic reaction occurs, and the potential is governed by the thermodynamic properties of the system. An excitation function (voltage) is applied, and a response function (current) is measured, with all other system variables held constant. The aim of the experiment is to obtain information (thermodynamic, kinetic, analytical, etc.) about the chemical system from observation of the excitation and response functions and knowledge of appropriate models for the system.¹⁵

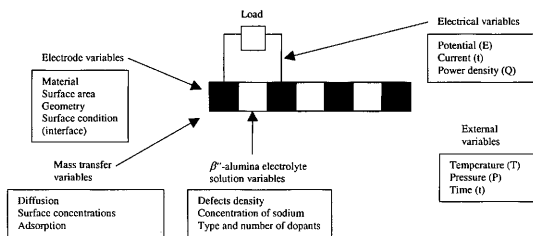


Figure 11. Variables affecting the rate of an electrode reaction in SETC electrode/electrolyte sample

Function structure of SETC

A function structure will aid in understanding the use of a SETC for testing electrode/electrolyte assemblies. It displays the functions that the SETC must provide in order to simulate AMTEC operating conditions and measure electrode characteristics.

Advantages of function structure are:

- Establishes the relationships among the functions
- Identifies interfaces among elements of the system
- Displays the entire system

A function structure enables us to classify the elements of the system in the experiment, and study them in a systematic manner. By breaking up functions into simpler subfunctions, we can subdivide a problem into more manageable parts and identify the variables that affect the measured parameters.

Since numerous functions are necessary in the experiment, it is helpful to classify these into top level and lower level functions. The number of such functions varies, depending on the degree of abstraction, or, conversely, on how close to physical functions they are.

As it was mentioned previously a SETC is used to simulate conditions of an actual AMTEC cell and measure the parameters characterizing AMTEC electrodes. The procedure for simulating AMTEC operating conditions and measuring electrode characteristics in the SETC must include a means for performing the following functions: (i) provide a means to control the AMTEC like conditions in the cell and (ii) provide a means to take measurements of the electrode characteristics. These functions and relationship among them are displayed in the function structure shown in Figure 12.

A function diagram is an organized display of the functions that must be performed to satisfy a need. It is organized such that the need is listed at the top of the diagram and the top level functions that must be performed or provided to meet the need are listed in the row just below the need. Below each function is a list of sub-functions that must be provided in order to perform that function. The sub-functions have lower level functions below them that must be provided to satisfy the sub-functions, and so on. The decomposition of the overall need into lower level functions continues until a level is reached at which no additional decomposition can be accomplished without designation of how the function will satisfied.

The functions at this level then become the initial functional requirements that must be satisfied to fulfill the need. That is, the initial functional requirements are what has to be provided in order to initiate the system design.

Upon completion of the function structure given in Figure 12 it was determined that in order to accurately simulate AMTEC operating conditions and measure electrode characteristics there are many functions that must be provided by the SETC. Two functions that thought to have a significant effect on the measurement of values for B and G (see section 1.3) highlighted in the function structure in Figure 12. The first of these is the control of the vapor pressure of the sodium source and the second is the configuration of the sample itself. The effect of the sodium vapor pressure may be determined by controlling the temperature of the sodium pool in SETC and the effect of sample configuration may be investigated testing various configurations of electrode/electrolyte samples. These two issues are discussed in detail in the subsequent sections.

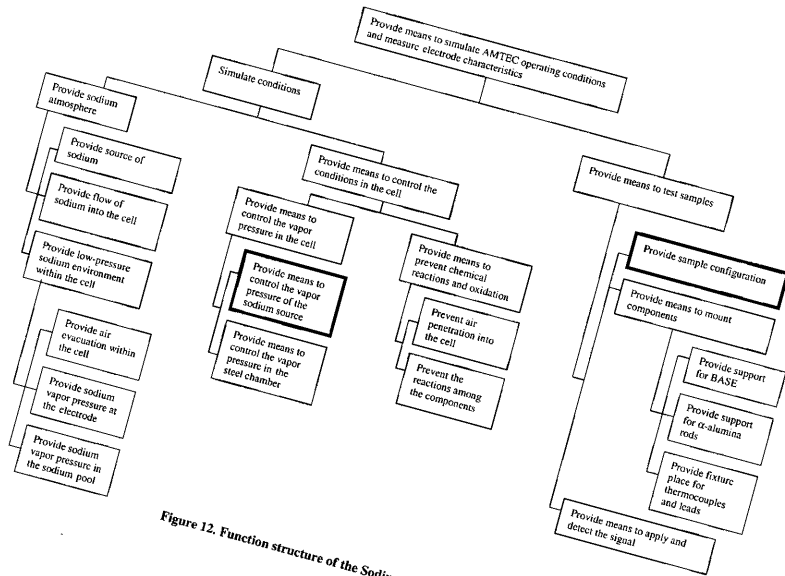


Figure 12. Function structure of the Sodium Exposure Test Cell (SETC)

3.1.1.2. Classification of Functions in the SETC Experiment

Basic functions are classified here under the following categories:

- Store/supply
- Connect
- Branch
- Channel
- Change magnitude
- Convert

All physical functions in SETC experiment can be shown to belong to one of these categories or to be a combination of some of them. A brief description of the basic functions is given below. The abbreviations given for each type will be used in the figures and in subsequent discussion.

- **STORE/SUPPLY (STSP)**. The function “store/supply” implies the storage, and eventual supplying, of material, energy, or signal. It includes the functions “store”, “empty”, “supply”, and “receive”, for energy, material, or signal. The functions “hold”, “stop”, and “release”, are also included under this basic function. Any of these can imply a lapse of time in execution of the “store/supply” function.
- **CONNECT (CONN)**. The function “connect” applies whether two or more quantities are brought together. It includes physical functions such as “mix”,

“switch”, or “compare” and arithmetic operations. The function has more than one input and one output.

- **BRANCH (BRCH)**. “Branch” is the opposite of the basic function “connect”. It has one input and more than one output. It includes functions such as “separate”, “cut”, or “count”.
- **CHANNEL (CHNL)**. The basic function “channel” includes physical functions such as “transmit”, “transport”, and “convey”. It applies to energy, material, or signal.
- **CHANGE MAGNITUDE (CHMG)**. The basic function “change magnitude” implies a change in magnitude while the form remains the same. It is used for energy or signal, and for material properties.
- **CONVERT (CVRT)**. “Convert” applies whenever the form of the output is different from that of the input, as in “convert” pressure to displacement. It can imply a change of state of a material or a change in the form of energy or signal.²⁸

In Figure 13 below the general schematic layout of SETC experimental setup is depicted. SETC experimental set up was broken up to several functions to better identify the error sources in SETC as well as to clarify the losses in the system. Each function represents some particular material, energy, and signal transport and serves as a link between two other functions. Figure 14 shows detail representation of functional layout of experimental setup. An explanation of each function is given in Appendix B of this work.

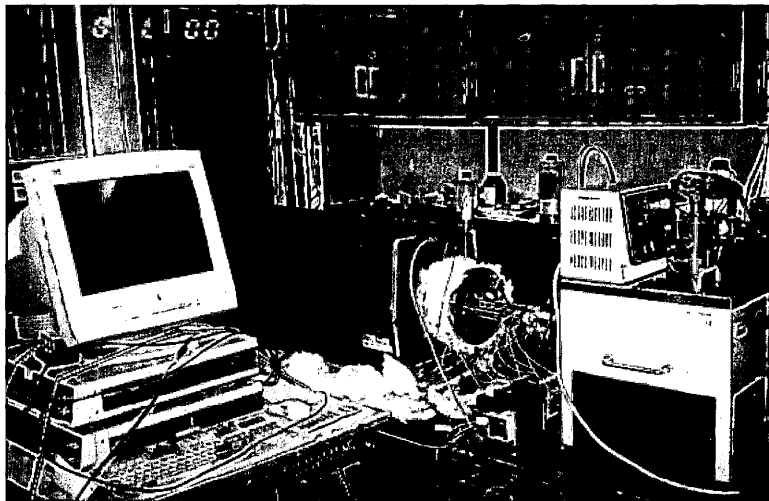
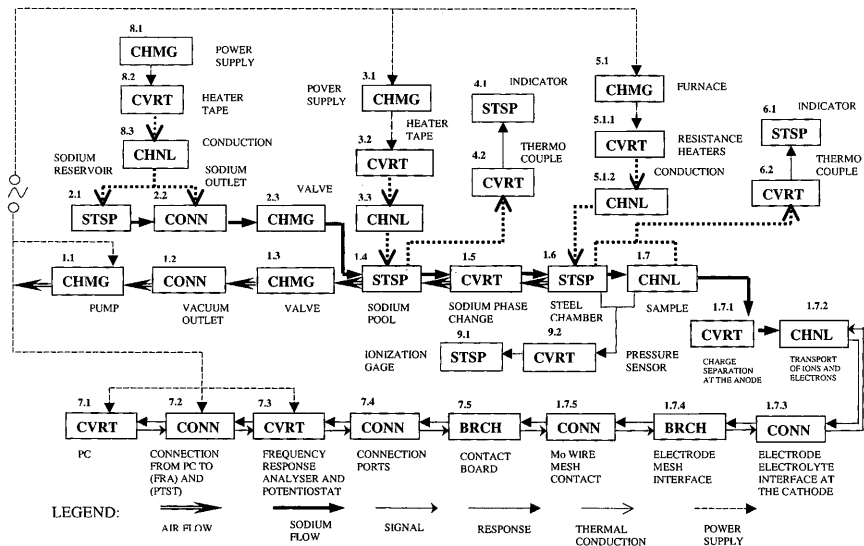


Figure 13. General view of the Sodium Exposure Test Cell experimental setup



3.2. Analysis of Tasks

This section gives a more in depth description of the effect of test conditions and sample configuration on the electrode/electrolyte measurements in a SETC. It gives a detail discussion about the identification of the accurate sodium vapor pressure correlation and a thermal finite element model of a SETC. In addition, this section explains the difference in sample configurations in SETC and AMTEC, and gives insights about different sodium ionic flow patterns in these configurations.

3.2.1. Effect of Sodium Vapor Pressure in the Sodium Exposure Test Cell on the Measurements of Electrode Characteristics

To determine the effect of the sodium vapor pressure in SETC on the measurements of electrode characteristics various sodium vapor pressure correlations at the required temperature range were considered and compared. The experiments were run at different sodium vapor pressures and the effect of these different pressure values was determined. In addition, the finite element model of SETC was developed which allowed identifying the temperature distribution within a SETC and understanding the nature of temperature gradients across the electrode/electrolyte assembly. This model will be able to indicate where the errors can occur in the experiments and helps us to improve the quality of measurements by controlling the sodium vapor pressure within a SETC.

3.2.1.1. Sodium Vapor Pressure Correlation in a Sodium Exposure Test Cell

As it is well known the measuring of the vapor pressures at different temperatures is a very difficult task. The sodium condenses on the pressure sensor and it does not allow obtaining accurate results from the measurements. The only way to obtain accurate vapor pressure values at different temperatures is to select the experimental values for known temperatures and correlate them with the values at required temperatures. Since the vapor pressure in general depends only on the temperature it is required to determine accurate correlation for the sodium vapor pressure in 250-350 °C range in SETC. The Clausius-Clapeyron equation suggests that vapor-pressure data might be fit reasonably well with an equation of the type²⁹

$$\ln P = A - \frac{B}{T} \quad [31]$$

where A is constant, T is the vapor temperature and $B = \frac{\Delta h}{R}$, Δh is the enthalpy change and R is gas constant. In order to maintain relatively high accuracy, the temperature range over which equation [31] is applicable is usually made relatively small. A modification of equation [31] can be made by noting that the critical temperature and pressure, as well as the normal boiling point T_b are easily measured. By using equation [30] at the critical point where $T = T_c$ and $P = P_c$ and at the normal boiling point at 1 atm we obtain an interpolating equation for the vapor pressure at any temperature between T and T_b .³⁰ At the normal boiling point $\ln P = 0$ and hence

$$\ln\left(\frac{P}{P_r}\right) = h^* \left(1 - \frac{1}{T_r}\right) \quad [32]$$

$$\text{and } h^* = T_{br} \left[\frac{\ln(P_r/1.013)}{1 - T_{br}} \right] \quad [33]$$

and the reduced temperatures, $T_{br} = T_b/T_c$ and $T_r = T/T_c$

To improve the accuracy of equation [30] over a wide range of temperature requires an increase in complexity of the equation. For example, the Clausius-Clapeyron equation is derived by assuming Δh is a constant. Over a wider temperature range we can model Δh as a linear function of temperature. This leads to a vapor-pressure temperature equation of the format³⁰

$$\ln P = A - \frac{B}{T} + C \ln T \quad [34]$$

Several different correlations exist that calculate the vapor pressure of sodium at different temperature ranges. In our experiments we used the correlation by Roger Williams (JPL)

$$P_{Na} = \frac{P_1(T_{Na} - 350)}{400} + \frac{P_2(750 - T_{Na})}{400} \quad [35]$$

where he selected two correlations for sodium vapor pressure at high temperature T_1 and low temperature T_2 , and interpolating found the correlation for the temperature range that is maintained in SETC, 250-350 °C. The correlation for high temperature is given by Ditchburn and Gilmour³¹

$$\log\left(\frac{P_1}{P_{atm}}\right) = 6.354 - \frac{5567}{T_{Na}} - 0.5 \log T_{Na} \quad [36]$$

(T in $^{\circ}\text{K}$ valid up to 1150 $^{\circ}\text{K}$)

The correlation for low temperature is given by Buck and Pauly³¹

$$\log\left(\frac{P_2}{P_{\text{torr}}}\right) = 8.08 - \frac{5479}{T_{\text{Na}}} \quad [37]$$

(T in $^{\circ}\text{K}$ valid at temperatures between the normal melting point and about 463 $^{\circ}\text{K}$).

In order to obtain the accurate values for the sodium vapor pressure, to calculate the normalized exchange current density, B , in SETC it is required to determine the correlation that is in agreement with experimental data and with other existed correlations at the required temperature range. In addition, it is required to determine an accurate temperature value for the sodium environment at 250-350 $^{\circ}\text{C}$ in SETC.

3.2.1.2. Thermal FEA Model of a Sodium Exposure Test Cell

An appropriate finite element model should accurately determine the temperature distribution within a SETC and across the BETA tube. Determination of the correct model will allow one to better understand the nature of temperature gradients in the cell and how these gradients can affect the controlling of vapor pressure, which in turn affects measured parameters, and therefore, correlate the values obtained from SETC with those of AMTEC cell.

3.2.2. Validation of the Electrode/Electrolyte Geometry in SETC

As previously mentioned, SETC is run to determine the performance of candidate electrodes for AMTEC without having to fabricate actual AMTEC cells.

Parameters such as B and G have been formulated to measure and compare the performance of the electrodes. A major difference between an SETC and AMTEC cell is the electrode/electrolyte configuration, as shown in Figure 16. SETC sample tubes have anode and cathode bands deposited on the outside of the electrolyte, both exposed to the same sodium vapor space. AMTEC tubes have the electrodes deposited on the inner and outer walls of the electrolyte, each exposed to a separate sodium vapor space.

During operation of an AMTEC cell each of the sodium ions encounters the same resistance, which produces a uniform current profile along the electrodes. In SETC the sodium ions on the edge of the anode opposite cathode encounter more ionic resistance than those atoms ionized closer to the cathode. This causes a non-uniform current profile across the anode and cathode.³² Figure 16 illustrates the fundamental geometry problem confronting SETC. In the former case (a), the bulk of the ion flow is in the axial direction, while in the latter case (b), the bulk of the ion flow is in the radial direction. If the ionic conductivity of BASE differs significantly between the two directions, the results measured in SETC will have little or no bearing on the performance of an electrode in an AMTEC cell. In addition, the geometry of the SETC sample allows possible ionic conductivity along the surface of the electrolyte, which is not possible in the AMTEC electrode/electrolyte configuration. Therefore, this is a source of inconsistency in SETC because non-uniform current profile within BASE affects B value.

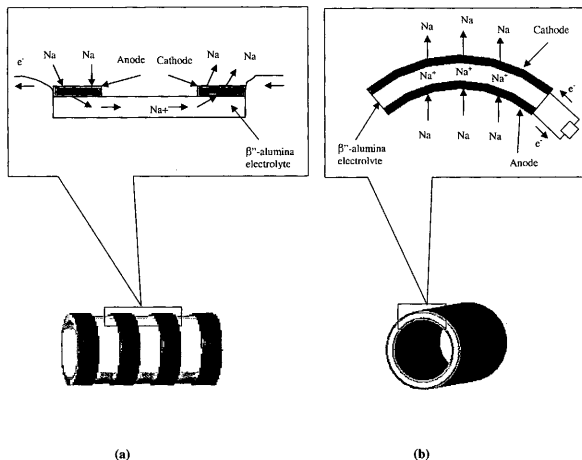


Figure 15. Schematic view showing the difference between an (a) SETC and (b) AMTEC electrode/electrolyte configuration

Sodium ions flow from the anode to the cathode in the small control volume of the AMTEC BETA tube, which can be approximated as a rectangular profile. If we assume that the sodium flow is uniform within the entire area of BETA tube then we can use simpler configuration of BASE in the experiment and obtain the parameters characterizing AMTEC electrodes performance. The configuration shown in figure 17 helps us identify differences in the apparent charge transfer resistances, R_{act} , of two

different electrode/electrolyte configurations. Running experiments in SETC, with both, configuration in figure 16 (a) and configuration in figure 17, and comparing the results it will be easy to conclude if there is a significant difference that can affect the measured parameters B and G . These differences can be determined from AC impedance measurements.

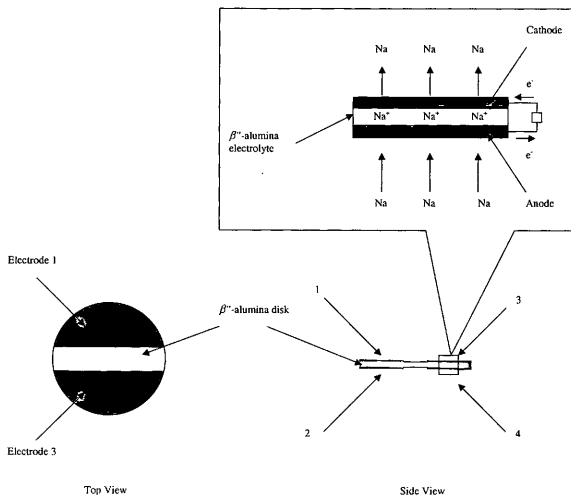


Figure 16. Schematic view of alternative electrode/electrolyte configuration in SETC

3.3. Experimental Procedure

In order to understand how the objective was met it is important to know how the procedure was developed at each step of the research.

The first part of the objective was to determine the effect of the source of inconsistency in measurements of sodium vapor pressure in the sodium pool of a SETC. This source of inconsistency addressed is the uncertainty of sodium vapor pressure value that is used in calculation of normalized exchange current density, B . This sodium vapor pressure value can be determined by selecting the accurate correlation for the sodium vapor pressure at the required temperature range in a SETC and by developing the finite element model to determine the temperature distribution in the sodium pool of a SETC.

It is clear that controlling the sodium vapor pressure in a SETC is a very important and difficult task, because even small gradients across the BASE sample and in the sodium pool can affect the measurements of B value and, therefore, the parameters of AMTEC cell performance.

In order to determine accurate values of the normalized exchange current density, B , which depends on the sodium vapor pressure of the sodium pool and vapor pressure at the sample, it is required to provide appropriate experimental conditions and to identify the accurate values of the sodium vapor pressure in the Sodium Exposure Test Cell. The sodium vapor pressure is a function of the sodium vapor temperature in the cell.

As it was explained in previous sections the steel chamber of a SETC is placed in the furnace and the manifold with the flow lines (sodium flow line and air flow line) is located outside in ambient temperature. The furnace is heated up and maintained at a

temperature of approximately 900°C . The sodium pool is wrapped by heater tapes and insulated all around. The power supply is used to maintain the temperature of sodium pool at about 300°C . The steel tubes for sodium and airflow and for α -alumina rods support are exposed to the ambient conditions with the temperature of about 25°C and steady convection coefficient $8-10\text{ W/m}^2\text{K}$.

To determine the accurate temperature distribution within SETC, ANSYS FEA code had been utilized and preliminary finite element model was developed. The flowchart of finite element modeling procedure is given in Figure 18. Two-dimensional model was selected to better simulate the thermodynamic conditions inside the SETC. Thermodynamic properties for three different areas in SETC model are given in Table 2.

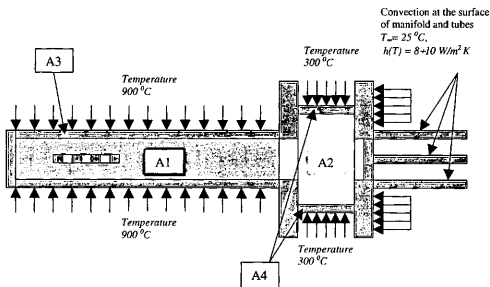


Figure 17. Schematic representation of applied thermal loads on SETC

Table 2. Selected thermodynamic properties with respect to the specified area for FEA analysis

	Specific Heat C_p (J/kg K)	Density ρ (kg/m ³)	Thermal conductivity k (W/m K)
A1- Sodium Vapor at 927 °C	2510	0.394	0.0483
A2- Sodium Vapor at 327 °C	1800	$2.63 * 10^{-3}$	0.03
A3- Stainless Steel at 927 °C	640	7900	28
A4- Stainless Steel at 327 °C	557	7900	19.8

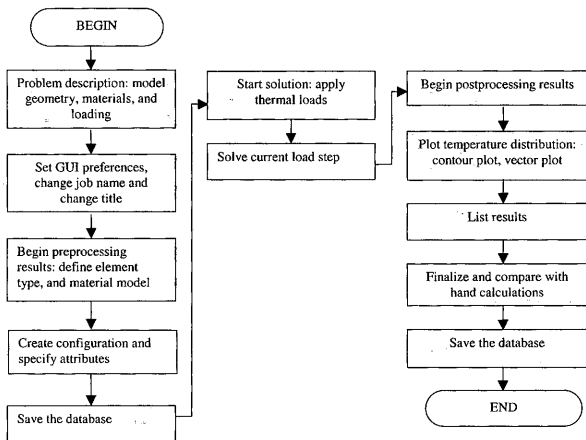


Figure 18. The flowchart of finite element modeling procedure in SETC

The second part of the objective was to determine if there was any difference in B value, at the equal electrode area, between BASE tube and BASE disk configuration.

Two 6.5mm diameter β'' -alumina disks and two BASE tubes from Ionotec Co., were sintered at the temperature 700^oC. Four molybdenum electrode patches and four molybdenum electrode bonds were deposited on β'' -alumina disk and tube respectively, using magnetron sputtering technique.

The air was pumped out from the chamber of magnetron sputtering machine to 0.9 torr (120 Pa). The chamber of the machine was flushed with argon to eliminate any existence of oxygen in it. The pressure inside the chamber, while flushing, was increased to 20 torr (2999 Pa) and the chamber again was pumped out to 0.9 torr (120 Pa). This procedure has been done for about 10 minutes. The gun power of magnetron sputtering machine was set up to 100 W. The real time to sputter molybdenum on the surface of β'' -alumina took about 10 minutes: 2 minutes for sputtering oxide level on the surface and 8 minutes for actual sputtering. The pressure inside the chamber during sputtering was maintained at about 9 torr (1200 Pa). Afterwards the molybdenum mesh was placed on each patch of an electrode and α -alumina rods were fixed on the mesh and were wrapped with the molybdenum wire on their sides. A sample of BASE tube 17.5 mm long, 6 mm in diameter and 1mm of the thickness of the β'' -alumina wall was used. Molybdenum electrodes with increments 2.5 mm were deposited by the same technique on the BASE and molybdenum mesh was wrapped around the electrodes and fixed with the molybdenum wire.

The samples were supported by α -alumina rods in SETC going through the flange into the steel chamber. Molybdenum leads were attached to each electrode band and threaded through electrically insulated feedthroughs at the flange. As it was mentioned previously the sodium β'' -alumina/electrode samples were heated in vacuum, as well as in low pressure sodium vapor, 10^{-7} to 10^{-6} torr (1.3×10^{-5} to 1.3×10^{-4} Pa) in SETC at temperature 850°C . Experiments were carried out using a high temperature furnace where SETC's steel chamber with a diameter of 76mm were placed. A turbo molecular pump and a rotary pump arranged in series were connected to the vacuum outlet of SETC to provide necessary low pressure inside the cell. After pumping out the air for about 20 hours and preheating the steel chamber up to the temperature 600°C and the sodium pool up to the temperature 300°C , the sodium reservoir with 20 grams of sodium in it was mounted into the sodium fill outlet. The sodium reservoir and sodium feedthroughs were heated up to the temperature 200°C using heater tapes for about half an hour to provide sodium flow into the sodium pool. Pressure was measured with an ionization gage attached to the vacuum outlet. The temperature at the samples and the temperature in the sodium pool were measured using thermocouples installed into the flange of SETC. After exposing samples in sodium environment in SETC for about 24 hours, measurements of Electrochemical Impedance Spectroscopy (EIS) and Current-Potential (IV) were taken. These values are necessary to calculate normalized exchange current density (B) and morphology factor (G), parameters explained previously, to characterize the performance of AMTEC electrodes.

CHAPTER IV

RESULTS AND DISCUSSION

This chapter consists of three sections. In the first section the introduction of results and measurement techniques used in the experiments are presented. In the second section the results of the experiments to determine the effect of the test conditions in a SETC on the electrode/electrolyte characteristics measurements are presented and some insights about errors that can occur in the experiment are given. In the third section the results of the investigation of the effect of the electrode/electrolyte geometry on the measurements are also presented and discussed.

4.1. Introduction of Results

As was mentioned previously, two types of measurements were made on electrode samples in the SETC, controlled potential current-voltage curves (iV curves) and Electrochemical Impedance Spectroscopy (EIS). The iV curves were created by applying a potential difference between two electrode bands or patches (depending on the sample geometry) and measuring the resulting current flow between them. Based on these curves, a limiting current, which is used in the calculation of G , can be measured. EIS is accomplished by applying a small potential, generally 5-10mV, to the electrode bands or patches and alternating the current initially at high frequencies, about 65kHz, reducing it in steps to low frequencies, about 0.1Hz. The resulting impedance is plotted on the complex plane producing a semi-circular curve with two real axis intercepts. The

difference between the high and low frequency intercepts is the apparent charge transfer resistance, R_{act} , of the electrode, which is a resistance including both charge transfer and sodium transport effects. The high frequency intercept value is the series resistance of the electrode, electrolyte and connecting leads. In this chapter the comparison of two different, previously mentioned configurations will be made. The values of the apparent charge transfer resistance, R_{act} , and limiting current, j_{lim} , will be considered, as the parameters affecting B and G values respectively, which in turn characterize AMTEC electrodes performance.

4.2. Effect of Sodium Vapor Pressure in SETC

The sodium vapor pressure in SETC directly affects the values of the normalized exchange current density, B , and dimensionless morphology factor, G . Therefore, the vapor pressure at the vapor source and sample had to be accurately known and maintained uniform. The vapor pressure is determined by measuring the temperature in the sodium vapor source. This necessitated that the temperature of the source be accurately known and uniform. This section discusses the approach followed to obtain accurate values of the vapor pressure in the sodium vapor source of the SETC. The first concern was to identify an accurate correlation between the sodium temperature and the sodium vapor pressure. This can be achieved by evaluating several different vapor pressure correlations and selecting one, which is consistent with other existing correlations and experimental data, and gives more accurate values over the extended temperature range. The second concern was to determine the uniformity of the sodium

temperature in the vapor source to insure that the temperature measurement of the sodium liquid pool was an accurate representation of the vapor source temperature to use in the correlation.

4.2.1. Evaluation of Sodium Vapor Pressure Correlations

After evaluating several correlations for the sodium vapor pressure in the sodium pool of SETC the following was concluded:

- 1) Roger Williams's correlation cannot be applied for temperatures above 980 °C.

In addition, this correlation gives greater values for the vapor pressure in the required temperature range 250⁰C-350⁰C, than other considered correlations

- 2) Ditchburn and Gilmore correlation fits very well for the required SETC sodium pool temperature range.³²
- 3) Buck and Pauly correlation gives values that are about twice as high as Ditchburn and Gilmore correlation at high temperatures.³²
- 4) New correlation was obtained by averaging Buck and Pauly correlation for lower temperatures and Browning and Potter correlation³³ for higher temperatures in order to obtain the vapor pressure values at the temperatures 250⁰C-350⁰C.

The result of the comparison of several existing evaluated sodium vapor pressure correlations and data is given in Figure 19.

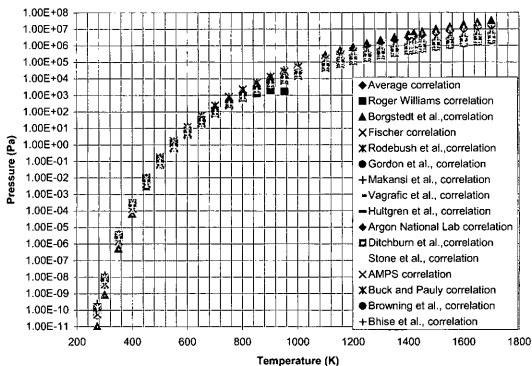


Figure 19. Comparison of different correlations and data for the sodium vapor pressure in the Sodium Exposure Test Cell

As it can be seen almost all correlations fit fairly well within the temperature range of about 300^0K - 800^0K . Explanation of all correlations and data for the sodium vapor pressure is given in Appendix D.

4.2.2. Evaluation of the Sodium Vapor Source Temperature Distribution in SETC

As it was mentioned previously, the finite element approach was chosen to determine the temperature distribution and thermal losses in SETC. The finite element model set up and selected properties were discussed in the Analysis of Tasks section of

this work. The objective of this analysis was to determine if heat transfer from the steel chamber in a SETC can affect the temperature distribution and therefore the temperature gradients in the cell. Two types of thermal loading conditions were used: (1) with convection from the hot end, manifold and steel tubes and insulation of the steel chamber area that is exposed to the ambient air; (2) the same conditions as in (1) but the insulation from the steel chamber area adjacent to the flange was removed and that area was exposed to the ambient conditions. Thermal loading conditions are depicted in Appendix C of this thesis.

As it was mentioned before the steel chamber of SETC was heated in the furnace and the manifold was exposed to the ambient air. The finite element thermal analysis showed that although the manifold and a part of steel chamber were exposed to the ambient conditions (condition 2) the temperature was uniform around the electrode sample. Even if some convective heat transfer was simulated at the hot end of the shell the results still indicated that there was not any temperature gradients across the sample. Figures 20-21 represent the difference in temperature profiles between two loading conditions. As you can notice the slope of the temperature curve in the region of the sodium vapor source for the condition (1) is approaching the maximum value then the slope of the temperature curve for the condition (2) in the same region. This can be explained that providing heat transfer from the steel chamber in the region adjacent to the manifold makes it possible to control the uniformity of the temperatures in the sodium vapor source. In addition, as you can notice this heat transfer does not affect the

uniformity of the temperature across the sample in the steel chamber. The detail description and steps of modeling is given in Appendix C.

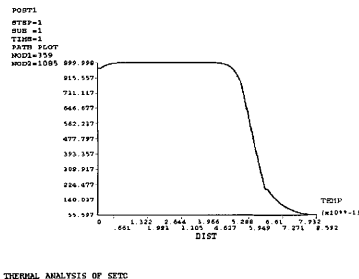


Figure 20. Graphical representation of the temperature distribution in a SETC with distance; condition (1)

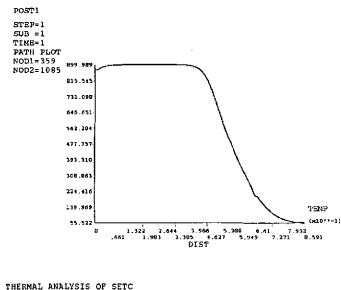


Figure 21. Graphical representation of the temperature distribution in a SETC with distance; condition (2)

4.3. Geometry Effect

The comparison of two different configurations of the electrode/electrolyte samples showed that there was little difference (about 10%) in calculated values of normalized exchange current density, B , and morphology factor, G . Although the ionic flow in the tube is along the surface of the electrolyte and ionic flow in the disk is through the bulk of the electrolyte, several measurements taken from the experiment confirm the fact that the apparent charge transfer resistance, R_{act} , and limiting current, j_{lim} , values did not change significantly for different electrode geometries. In addition, several measurements of R_{act} and j_{lim} have been done between different electrode pairs on the disk and finally confirmed the fact that the geometry of the sample in a SETC does not have a significant effect on the results of the experiment.

The measurements were done using 3-point measurement technique at various temperatures of the electrode and sodium vapor source.

Since the tube samples did not behave properly (readings were very erratic) it was impossible to obtain the values of limiting current, j_{lim} , for this configuration. The data for j_{lim} were obtained applying voltage between different electrode pairs only for the BETA disk.

Figures 22-25 represent the Electrochemical Impedance Spectroscopy (EIS) measurements for tube and disk configurations at various temperatures of the electrode sample and the sodium vapor source. From these plots the apparent charge transfer resistance, R_{act} , can be determined. As it was mentioned previously the apparent charge

transfer resistance is the difference between the values of high frequency intercept and low frequency intercept on the EIS plot.

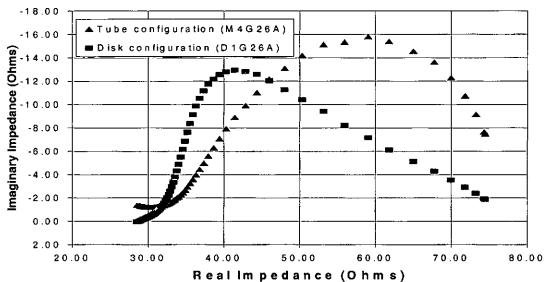


Figure 22. EIS plot of 3-probe measurements for the tube and disk configuration; Temperature at the electrode 562 °C. Temperature in the sodium pool 193 °C

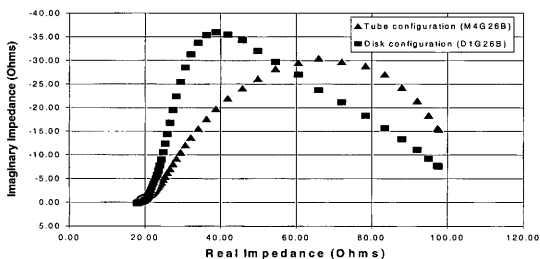


Figure 23. EIS plot of 3-probe measurements for the tube and disk configuration; Temperature at the electrode 698 °C. Temperature in the sodium pool 230 °C

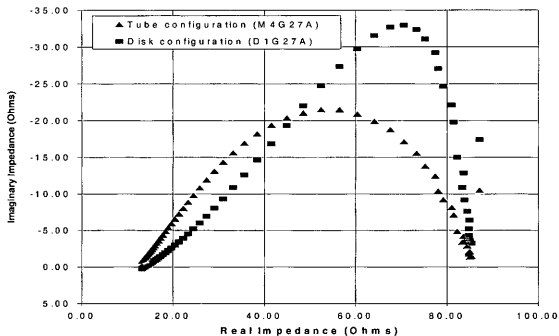


Figure 24. EIS plot of 3-probe measurements for the tube and disk configuration; Temperature at the electrode 811 °C. Temperature in the sodium pool 271 °C

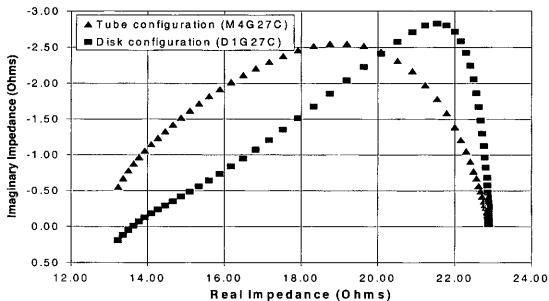


Figure 25. EIS plot of 3-probe measurements for the tube and disk configuration; Temperature at the electrode 861 °C. Temperature in the sodium pool 299 °C

As was mentioned the measurements of the limiting current, j_{lim} , between electrode pairs on the disk were determined from iV curves. iV curves for different electrode pairs on the disk sample show that the limiting current does not change considerably for all measured temperature ranges. From limiting current value of morphology factor, G , can be obtained which characterizes the sodium transport in the electrode. Figures 26 to 31 represent iV curves for different electrode pairs on the disk.

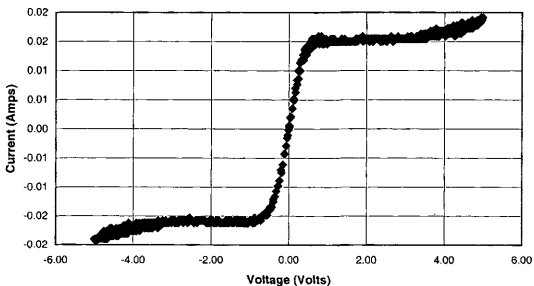


Figure 26. iV curve for the disk configuration between electrodes 1-2

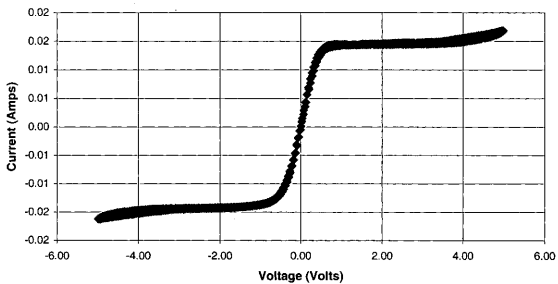


Figure 27. IV curve for the disk configuration between electrodes 1-3

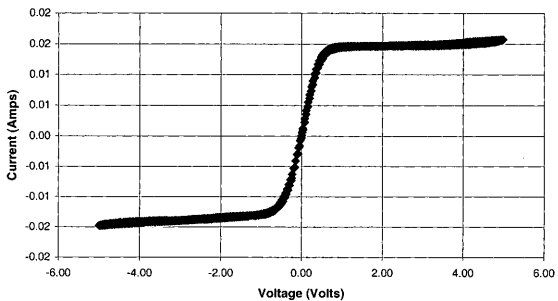


Figure 28. IV curve for the disk configuration between electrodes 1-4

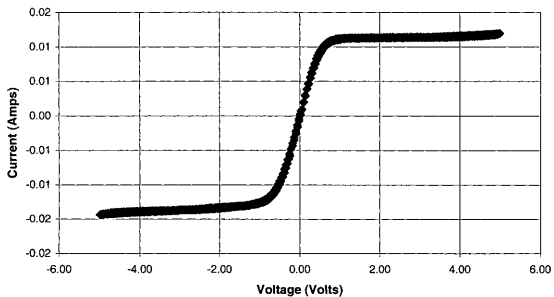


Figure 29. IV curve for the tube configuration between electrodes 2-3

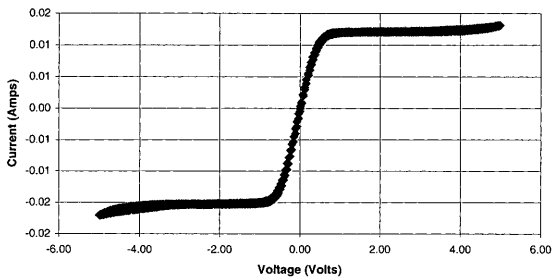


Figure 30. IV curve for the disk configuration between electrodes 2-4

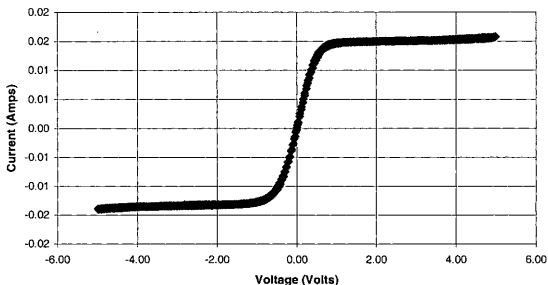


Figure 31. IV curve for the disk configuration between electrodes 3-4

A comparison of values, characterizing the performance of electrode/electrolyte assembly, for two different geometries is given in the Tables 3 to 6. It can be seen that at temperatures of the electrode 562°C , 698°C , and 811°C the normalized exchange current density values for the disk configuration are less than those for the tube configuration. The values of the apparent charge transfer resistance, R_{act} , on the contrary, are greater for the disk configuration than those for the tube configuration. For the temperature at the electrode 861°C , the normalized exchange current density, B , for the disk configuration is still less than that for the tube configuration, but the apparent charge transfer resistance, R_{act} , for the disk configuration is also less than that for the tube configuration. The following tables show the comparison of the parameters measured in the SETC experiment for various temperatures of the electrode and sodium vapor source.

**Table 3. Parameters measured in SETC for two different electrode/electrolyte configurations.
Temperature at the electrode 562 °C. Temperature in the sodium pool 193 °C**

	$R_{act}(ohms)$	$j_{lim}(amps)$	B	G
<i>BASE Tube (molybdenum electrode) (M4G26A)</i>	46.3	---	114.9	---
<i>BASE Disk (molybdenum electrode) (D1G26A)</i>	48	1.43E-2	89.7	---

**Table 4. Parameters measured in SETC for two different electrode/electrolyte configurations.
Temperature at the electrode 698 °C. Temperature in the sodium pool 230 °C**

	$R_{act}(ohms)$	$j_{lim}(amps)$	B	G
<i>BASE Tube (molybdenum electrode) (M4G26B)</i>	81	---	11.3	---
<i>BASE Disk (molybdenum electrode) (D1G26B)</i>	95.9	1.44E-2	7.6	9.1

**Table 5. Parameters measured in SETC for two different electrode/electrolyte configurations.
Temperature at the electrode 811 °C. Temperature in the sodium pool 271 °C**

	$R_{act}(ohms)$	$j_{lim}(amps)$	B	G
<i>BASE Tube (molybdenum electrode) (M4G27A)</i>	72	---	3.2	---
<i>BASE Disk (molybdenum electrode) (D1G27A)</i>	91.4	1.46E-2	2	98.7

**Table 6. Parameters measured in SETC for two different electrode/electrolyte configurations.
Temperature at the electrode 861 °C. Temperature in the sodium pool 299 °C**

	$R_{act} (ohms)$	$j_{lim} (amps)$	B	G
<i>BASE Tube (molybdenum electrode) (M4G27C)</i>	9.7	---	11.5	---
<i>BASE Disk (molybdenum electrode) (D1G27C)</i>	8.9	1.49E-2	10	304

Measured apparent charge transfer resistance, R_{act} , values for one set of measurements is shown in Table 7. The sodium vapor source temperature was 299-301°C, measured with a thermocouple in the sodium pool in the SETC. The electrode sample temperature was 864-866°C, measured 5 cm away from the position of the samples. Configuration 1-2 has electrode 1 as the working electrode and reference 1, with electrode 2 as the counter electrode, and electrode 4 as reference 2, see Figure 16. Configuration 1-3, Figure 16, has electrode 1 as the working electrode and reference 1, with electrode 3 as the counter electrode, and electrode 4 as reference 2. Configuration 1-4 has electrode 1 as the working electrode and reference 1, with electrode 4 as the counter electrode, and electrode 2 as reference 2.

Table 7. R_{act} values measured in SETC for different electrode pairs on the disk at the temperature of the electrode 861^oC

Electrode Pair	R_{act} (ohms) 8/27/01	R_{act} (ohms) 8/28/01	R_{act} (ohms) 8/29/01	R_{act} (ohms) 8/30/01
1-2	9.0	9.4	9.0	9.7
1-3	9.2	9.9	9.3	10.1
1-4	8.7	9.6	---	9.8
2-3	7.2	8.5	---	8.4
2-4	7.8	8.14	7.55	8.1
3-2	18.6	28	---	33
3-4	18.7	22	19.9	31.6
4-1	10.9	11.9	---	11.9

Measured limiting current values, j_{lim} , for two sets of measurements are shown in Table 8. Configuration 1-2 is identical to the sodium ion flow configuration in an AMTEC converter. Configuration 1-3 is identical to the sodium ion flow configuration in a SETC. Configuration 1-4 is intermediate between the configurations 1-2 and 1-3. Note that the fluctuations from day to day are greater than the differences between the configurations. Also, the trends in the values of R_{act} and j_{lim} are consistent between configurations.

Table 8. j_{lim} values measured in SETC for different electrode pairs on the disk at the temperature of the sample electrode 861^oC

Measured electrode (Electrode Pairing)	j_{lim} (milliamps) 08/31/01	j_{lim} (milliamps) 09/04/01	j_{lim} (milliamps) 09/04/01	j_{lim} (milliamps) 09/07/01
1 (1-2)	15.8	14.3	13.8	13.4
1 (1-3)	15.6	14.2	13.6	13.2
1 (1-4)	---	14.1	13.7	13.2
2 (1-2)	15.4	14.5	14.7	15.1
2 (2-3)	---	14.4	14.6	14.8
2 (2-4)	15.2	14.3	14.7	14.8
3 (3-4)	12.2	11.4	11.6	11.7

Figures 32 to 35 below were compiled from B values calculated using electrode temperature, sodium vapor source temperature and apparent charge transfer resistance values measured in the SETC for the two different sample configurations. Each plot represents a different electrode on a sample for each of the configurations (see Figures 15 and 16). The trend line superimposed on the data plot comes from a polynomial regression using all data points. These are plots of B value versus the electrode temperature. As expected little variations exist between different sample configurations, and also between electrode pairs.

As seen in Figures 32-35, the value of B in general decreases with increasing electrode temperature, but increases for both configurations and each electrode at the temperature of 861^oC. The general relation between trend lines of two different

configurations of each electrode indicates the steady change of B value with change of electrode temperature.

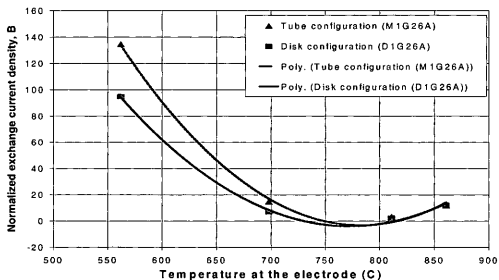


Figure 32. Polynomial trends of B value with respect to the electrode temperature for the tube and disk configuration for electrode 1

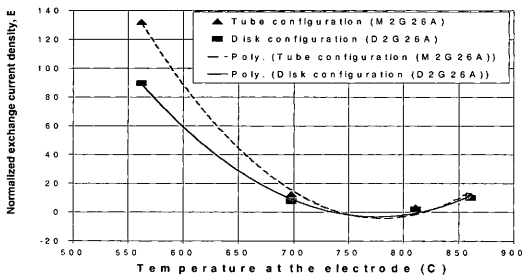


Figure 33. Polynomial trends of B value with respect to the electrode temperature for the tube and disk configuration for electrode 2

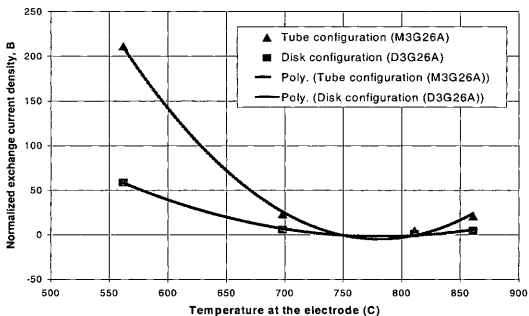


Figure 34. Polynomial trends of B value with respect to electrode temperature for the tube and disk configuration for electrode 3

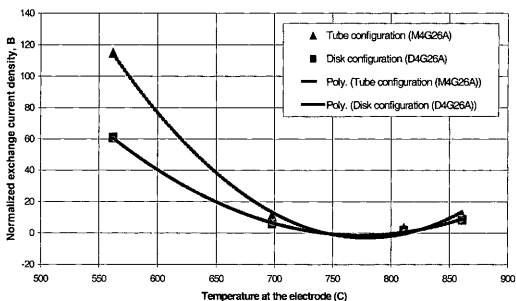


Figure 35. Polynomial trends of B value with respect to electrode temperature for the tube and disk configuration for electrode 4

As it was discussed in previous chapters sodium ions move along the surface of the β'' -alumina in the tube configuration in a SETC, rather than through it as in disk configuration. This flow pattern would encourage sodium ions to react preferentially at sites near the inner edges of each electrode, particularly at lower vapor pressure conditions, when many sites are not constantly occupied. As the sodium vapor pressure increases, more current is pushed through the bulk of the sample, so more and more sites are constantly occupied, forcing the additional sodium ions to use more distant sites to react. Eventually, entire area of the electrode would be in constant use, and the value of B would no longer change with temperature.

Notice that the difference in B value for the two configurations decreases as the temperature increases toward actual AMTEC temperatures. This again indicates that the geometry of the sample will not affect the electrode characteristics determined in a SETC. There appears that there is a tendency for B value to increase after decreasing with temperature and reaching a minimum. This trend, however, is inconclusive without data at higher temperatures.

CHAPTER V

FINDINGS, CONCLUSION AND RECOMMENDATIONS

5.1. Summary

Sodium exposure tests were conducted to determine if the parameters measured within a Sodium Exposure Test Cell (SETC) provide an effective predictor of actual AMTEC electrode performance. Two different electrode/electrolyte configurations were used to determine the difference in the apparent charge transfer resistance, R_{act} , and limiting current j_{lim} , of electrodes. These values were measured by controlled potential current-voltage curves (iV curves) and Electrochemical Impedance Spectroscopy (EIS) techniques.

To validate the accuracy of the sodium vapor pressure value in the sodium pool, several sodium vapor pressure correlations were considered and compared at the required temperature range in SETC, and Ditchburn and Gilmore correlation was selected. In addition, to determine the inconsistency in the temperature measurements in the sodium pool the finite element modeling was done to identify the temperature distribution and temperature gradients in SETC.

In order to identify the errors and inconsistencies in SETC experimental setup, the function structure was developed, and functional requirements of every function were determined. The errors in the experiment can occur because of the current collector overlap or underlap on the electrode, the presence of vacuum leak and inconsistency to sense accurately the sodium vapor pressure in the sodium pool. Since the relationship

between sodium pool temperature and sodium vapor pressure is exponential, even a 10°C difference between the measured sodium pool temperature and the actual sodium pool temperature causes a 20% to 30% change in the calculated value of B .

5.2. Findings

The important findings from this investigation are shown below:

- Ditchburn and Gilmour correlation for the sodium vapor pressure was the best correlation suggested to be used in calculations of the sodium vapor pressure in a SETC.
- Uninsulated region of the steel chamber of a SETC made it possible for heat to be transferred from that region which affected the temperature to be uniform in the sodium vapor source in a SETC.
- All configurations of electrode/electrolyte sample tested in a SETC have shown little difference in B and G values and had the same trend in decreasing a difference in B value between the two configurations as the temperature increased toward actual AMTEC temperatures.

5.3. Conclusion

The attempts made in this research, to identify accurate correlation for the sodium vapor pressure and to maintain the uniformity of the temperature in the sodium vapor source, show that it is possible to accurately simulate AMTEC like conditions in a SETC and therefore to obtain accurate values of B and G that characterize the performance of AMTEC electrodes.

The results of this research also indicate that the geometry of the sample in SETC does not have a significant effect on the results of the experiment. Further, both configurations, SETC BASE tube, and SETC BASE disk, clearly showed the same trend in the measured values. This indicates the fact that the SETC configuration used by JPL and Center for Space Power in the past gave useable data for calculating the AMTEC electrode parameters B and G , and may be confidently used for measuring AMTEC electrode performance in the future.

5.4. Recommendations

Further consider small changes in the apparent charge transfer resistance, R_{act} , and limiting current j_{lim} , and determine the deviation from the AMTEC electrode/electrolyte configuration.

Find correlation between axial ionic flow in the disk configuration in SETC and radial ionic flow in electrode/electrolyte configuration in AMTEC cell.

Find better ways to fix the current collector on the disk, and try to minimize parasitic losses related to active electrode area.

Develop a detail function structure for electrode operation and try to identify losses in the experiment.

Run experiments in SETC at higher temperatures, about 1000⁰C of electrode temperature and 400⁰C of the sodium pool temperature, and determine if there is any change in B value. Also determine if there is any Knudsen flow effect on the measured parameters.

Continue investigations in determining accurate value of the sodium vapor pressure in the sodium pool. Try to simulate accurate sodium vapor properties at the required temperature range in SETC and develop consistent thermal model to determine the temperature distribution in SETC.

REFERENCES

1. J. W. Suito, M. Shirbacheh, R. M. Williams, C. P. Bankston, *AMTEC Technology Development Plan*, JPL, 1 (September 1990)
2. R. D. Cockfield, E. W. Tobery, in *Proceedings of the Space Technology and Applications International Forum*, 1482-1487, (2000).
3. J. Tournier, M. S. El-Genk, in *Proceedings of the 33rd Intersociety Energy Conversion Engineering Conference*, paper 98-057, ANS, Colorado Springs, CO (1998)
4. C. S. Mayberry, J. Merrill, D. Radzykewycz, K. Reinhardt, *Renewable Energy*, **23**, 451-461, (2001).
5. A. K. Hyder, R. L. Wiley, G. Halpert, D.J. Flood, S. Sabripour, *Spacecraft Power Technologies*, Imperial College Press, London (2000).
6. M. A. Ryan, V. B. Shields R.H. Cortez, L. Lara, M. L. Homer, R. M. Williams, in *Proceedings of the Space Technology and Applications International Forum*, 1377-1382, (2000).
7. J. M. Tournier, M. S. El-Genk, *Energy Conversion & Management*, **40**, 139-173, (1999).
8. M. A. Ryan, R. M. Williams, L. Lara, R. H. Cortez, M. L. Homer, V. Shields, J. Miller, and K. S. Manatt, in *Proceedings of the 33rd Intersociety Energy Conversion Engineering Conference*, paper 98-335, ANS, Colorado Springs, CO (1998)
9. R. M. Williams, M. E. Loveland, B. Jeffries-Nakamura, M. L. Underwood, C. P. Bankston, H. Leduc, and J. T. Kummer, *J. Electrochem. Soc.*, **137**, 1709 (1990).
10. A. Schock, H. Noravian, C. Or, V. Kumar in *Proceedings of the Space Technology and Applications International Forum*, 1534-1554 (1999).
11. E. H. Kennard, *Kinetic Theory of Gases*, pp. 69 and 304, McGraw-Hill, New York (1938).
12. T. Kudo, K. Fueki, *Solid State Ionics*, Kodansha Ltd., Tokyo (1990).
13. M. A. K. Lodhi, A. Daloglu, *J. Power Sources*, **93**, 32-40, (2001).

14. N. Weber, *Energy Conversion*, **14**, 1 (1974).
15. A. J. Bard, L. R. Faulkner, *Electrochemical Methods: Fundamentals and Applications*, John Wiley & Sons, New York (1980).
16. R. M. Williams, B. Jeffries-Nakamura, M. L. Underwood, C. P. Bankston, and J.T. Kummer, *J. Electrochem. Soc.*, **137**, 1716 (1990)
17. T. Kummer, *Beta-Alumina Electrolytes*, Progress in Solid State Chemistry, Vol.7, p.141, Pergamon Press Inc., New York (1972).
18. J.L. Sudworth, A.R. Tilley, *The Sodium Sulfur Battery*, Chapman and Hall, New York (1985).
19. S. Geller, *Solid Electrolytes*, Springer-Verlag, Berlin (1977).
20. C. Subbarao, *Solid Electrolytes and Their Applications*, Plenum Press, New York (1980).
21. R. M. Williams, M. A. Ryan, M. L. Homer, L. Lara, K. Manatt, V. Shields, R.H. Cortez, J. Kulleck, in *Proceedings of the 33rd Intersociety Energy Conversion Engineering Conference*, paper 98-333, ANS, Colorado Springs, CO (1998).
22. R. M. Williams, M. L. Homer, J. Kulleck, L. Lara, A. K. Kisor, R.H. Cortez, V. B. Shields, M. A. Ryan, in *Proceedings of the Space Technology and Applications International Forum*, 1408-1411, (2000).
23. H. Yokokawa, T. Horita, N. Sakai, T. Kawada, M. Dokiya, *Solid State Ionics*, **78**, 203-210, (1995).
24. B. Fiebig, M. Schuller, M. Ryan, R. Williams, P. Hudson, in *Proceedings of the Space Technology and Applications International Forum*, 99-105 (1999).
25. R.M.Williams, M.L.Homer L.Lara R.H.Cortez J.Miller B.Jeffries-Nakamura M.L.Underwood, A.Kisor, V.B.Shields K.S.Manatt M.A.Ryan, in *Proceedings of the 33rd Intersociety Energy Conversion Engineering Conference*, paper 98-332, ANS, Colorado Springs, CO (1998).
26. R. M. Williams, B. L. Wheeler, B. Jeffries-Nakamura, M. Loveland, C. P. Bankston, T. Cole, *J. Electrochemical Society*, **135**, 2736-2742, (1988).

27. R. M. Williams, M. A. Ryan, H. LeDuc, R.H. Cortez, C. Saipetch, V. B. Shields, K. S. Manatt, M. L. Homer, in *Proceedings of the 33rd Intersociety Energy Conversion Engineering Conference*, paper 98-000, ANS, Colorado Springs, CO (1998).
28. M. S. Hundal, *Systematic Mechanical Designing: A Cost and Management Perspective*, ASME Press, New York (1997).
29. K. Wark, *Advanced Thermodynamics for Engineers*, McGraw-Hill, Inc., Boston (1995).
30. J. W. Tester, M. Modell, *Thermodynamics and Its Applications*, 3rd Edition, Prentice-Hall, Inc., Upper Saddle River, NJ (1997).
31. O. J. Foust, *Sodium-NaK Engineering Handbook*, Vol. I, pp. 56-59, Gordon and Breach Science Publishers, New York (1972).
32. M. Schuller, B. Fiebig, P. Hadson, A. Williams, in *Proceedings of the Space Technology and Applications International Forum*, paper AIAA-2000-2927. (2000).
33. J. K. Fink, L. Leibowitz, *Thermodynamic and Transport Properties of Sodium Liquid and Vapor*, pp. 55-63, Argonne National Laboratory, ANL/RE-95/2, Argonne, IL (1995).
34. F. P. Incropera, D. P. DeWitt, *Fundamentals of Heat and Mass Transfer*, John Wiley & Sons, New York (1996).
35. D. L. Logan, *A First Course in the Finite Element Method*, PWS Publishers, Boston (1986).
36. ANSYS Training Manual for Release 5.7, *Heat Transfer*, ANSYS, Inc., PA(2001).
37. H. U. Borgstedt, C. K. Mathews, *Applied Chemistry of the Alkali Metals*, Plenum Press, New York (1987).
38. A. K. Fischer, *The Review of Scientific Instruments*, **37**, 717 (1966).
39. F. Petiot, J. M. Seiler, *High Temperatures-High Pressures*, **16**, 289-293, (1984).
40. R. W. Ohse, *Handbook of Thermodynamic and Transport Properties of Alkali Metals*, Blackwell Scientific Publications, Oxford (1985).
41. M. M. Makansi, C. H. Muendel, W. A. Selke, *J. Chem. Phys.* **59**, 40 (1955).
42. J. Bohdanský, H. E. J. Schins, *J. Physical Chemistry*, **71**, 215, (1967).

APPENDIX A

ELECTROCHEMICAL MEASUREMENTS FOR AMTEC ELECTRODES

Electrochemical Impedance Spectroscopy

Electrochemical Impedance Spectroscopy is a valuable technique. It is widely used in different research areas. The method involves the application of a small perturbation of the potential or the current. The perturbation is a single sine wave or a superposition of a number of sine waves with different frequencies. From the applied perturbation and its measured response the magnitude of the impedance and phase shift is determined. Since the technique is called spectroscopy, parameters are measured as a function of the frequency of the applied perturbation.

Theory

Ohm's law gives a simple relation between dc-potential (E) and dc-current (i):

$$E = iR$$

When ac-signals are involved the relation is:

$$E_{ac} = i_{ac}Z$$

where Z is the impedance

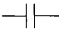
Basic elements and plot formats

The simplest case is found with a pure resistance

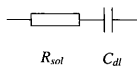
Resistance:  $Z=R$

The impedance is $Z = R$. The phase difference between the ac-potential and ac-current is 0. The impedance of a resistance is independent of the applied frequency.

The capacitor is also an important element in electrochemical impedance spectroscopy. The interface between the electrode and solution ideally behaves as a capacitor and is called electrical double layer capacitance. The magnitude of the impedance of a capacitor is equal to $\frac{1}{\omega C}$, and the phase angle is always 90° .

Capacitance:  $Z = \frac{1}{\omega C}$

The most simple electrochemical cell behaves like a resistance in series with a capacitor.



R_{sol} is the ohmic resistance of the solution and C_{dl} the double layer capacitance. At high frequencies, the magnitude of the impedance equals R_{sol} with a phase angle of 0° . At low frequencies the impedance will be frequency dependent and the phase angle will be 90° .

The complex plane notation is depicted in Figure 36.

$$Z = Z' + jZ'' \quad \text{with } j = \sqrt{-1}$$

The value Z' is the projection along the x-axis and Z'' along the y-axis. Z' is called in-phase or real impedance and Z'' out-of-phase or imaginary impedance. The cell impedance is:

$$|Z| = (Z'^2 + Z''^2)^{1/2} \quad \text{and} \quad \tan \phi = \frac{Z''}{Z'}$$

The complex notation of the impedance of the cell is given by:

$$Z = R_{sol} - \frac{j}{\omega C_{dl}}$$

Due to the double layer capacitance the cell impedance usually depends on the applied frequency. The value of Z' is independent of the frequency and is equal to R_{sol} , while the imaginary impedance Z'' equals $\frac{1}{\omega C}$.

Another common plot format of impedance spectra is the Bode plot. In general it depicts two curves. The x-axis shows the logarithm of the frequency. The left axis gives the logarithm of the impedance, while the right axis the phase angle. If a faradaic reaction occurs at the electrode, a faradaic impedance parallel to the double layer will be found. In case of a simple irreversible reaction, this faradaic impedance is a pure resistance and is called charge transfer resistance R_{ct} .

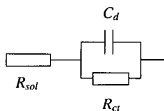


Figure 36. Equivalent circuit for a simple electrochemical cell, showing the solution resistance R_{sol} , double layer capacitance C_{dl} and charge transfer resistance R_{ct}

This circuit will show a semi-circle in the impedance plot. At high frequencies the impedance is determined by the solution resistance R_{sol} . At very low frequencies the cell impedance is equal to $R_{sol} + R_{ct}$. Both limits show a phase shift equal to 0° . At

intermediate frequencies, the cell impedance is influenced by the value of the double layer capacitance C_{dl} .

APPENDIX B

DESCRIPTION OF FUNCTIONS IN SETC EXPERIMENTAL SETUP

- **STORE/SUPPLY (STSP).** The function “store/supply” implies the storage, and eventual supplying, of material, energy, or signal. It includes the functions “store”, “empty”, “supply”, and “receive”, for energy, material, or signal. The functions “hold”, “stop”, and “release”, are also included under this basic function. Any of these can imply a lapse of time in execution of the “store/supply” function.
- **CONNECT (CONN).** The function “connect” applies whether two or more quantities are brought together. It includes physical functions such as “mix”, “switch”, or “compare” and arithmetic operations. The function has more than one input and one output.
- **BRANCH (BRCH).** “Branch” is the opposite of the basic function “connect”. It has one input and more than one output. It includes functions such as “separate”, “cut”, or “count”.
- **CHANNEL (CHNL).** The basic function “channel” includes physical functions such as “transmit”, “transport”, and “convey”. It applies to energy, material, or signal.
- **CHANGE MAGNITUDE (CHMG).** The basic function “change magnitude” implies a change in magnitude while the form remains the same. It is used for energy or signal, and for material properties.

- **CONVERT (CVRT)**. “Convert” applies whenever the form of the output is different from that of the input, as in “convert” pressure to displacement. It can imply a change of state of a material or a change in the form of energy or signal.²⁸

An explanation of each function is given below.

- 1.1 **CHMG – Pump**. This function provides a means to move air from the Sodium Exposure Test Cell and provides vacuum of 10^{-7} torr in the steel chamber of SETC.
- 1.2 **CONN – Vacuum outlet**. This function provides proper connections of the pump outlet to SETC. The joint between pump outlet and SETC vacuum outlet must be sealed good enough to prevent air penetration into SETC.
- 1.3 **CHMG – Valve**. This function controls airflow rate from SETC. This valve controls the sealing of SETC’s vacuum outlet.
- 1.4 **STSP – Sodium pool**. This function provides a means to contain the sodium that is coming from sodium reservoir. Sodium pool contains sodium within specified place preventing liquid sodium flow in the steel chamber.
- 1.5 **CVRT – Sodium phase change**. This function provides means to change the phase of sodium from liquid to vapor in the sodium pool. The sodium pool is heated to the temperature of about 300° C and sodium inside it evaporates and moves to the sample in the steel chamber.

- 1.6 *STSP – Steel chamber.* This function provides means to contain sodium vapor and accommodate the samples in the vapor sodium environment.
- 1.7 *CHNL – Electrode/electrolyte sample.* This top-level function provides means for all physical and electrical processes at the β' -alumina electrolyte, electrode/electrolyte interface, and electrode.
- 1.7.1 *CVRT – Charge separation at the anode.* This function provides means to separate the charge at the anode. Potential difference applied to the electrodes initializes charge transfer and mass transport within electrode/electrolyte assembly and charge separation takes place in the electrode/electrolyte interface.
- 1.7.2 *CHNL – Transport of ions and electrons.* This function provides means to carry electron current through the leads and sodium ion current through the electrolyte.
- 1.7.3 *CHNL – Cathode/electrolyte interface.* This function provides means for processes taking place in cathode/electrolyte interface. These processes include charge transfer across the interface, mass transport, recombination of sodium ions and electrons and chemical kinetics. The value that is measured showing the resistance at the interface is the normalized exchange current density, B .

- 1.7.4 *BRCH – Electrode/mesh interface.* This function provides means to carry the current from the electrode. Molybdenum mesh is bounded around the electrode to provide better contact between electrode and leads going to FRA and PTST.
- 1.7.5 *CONN – Mo wire/mesh contact.* This function provides means to fix the current collector on the electrode and to carry the current through the leads. The contact resistance between wire and mesh should be minimized.
- 2.1 *STSP – Sodium reservoir.* This function provides SETC with sodium source. The sodium is stored in the steel container, which has an outlet cap nut that prevents sodium oxidation while keeping the container in the ambient conditions.
- 2.2 *CONN – Sodium outlet.* This function provides means for sodium to flow in the SETC sodium pool. It is very important to provide good sealing in the joints to prevent sodium leak and oxidation of sodium.
- 2.3 *CHMG – Sodium outlet valve.* This function provides means to control sodium flow rate into SETC. This valve controls the sealing of SETC's sodium outlet.
- 3.1 *CHMG – Power Supply.* This function provides energy source in order to heat the sodium pool.
- 3.2 *CVRT-Heater Tape.* This function provides means to convert electricity into thermal energy in order to heat sodium pool to the temperature of

- 300 °C. The heater tape is banded around sodium pool and connected to the power supply.
- 3.3 *CHNL – Conduction.* This function provides means to transfer the thermal energy from heater tape to the sodium pool.
- 4.1 *STSP – Indicator.* This function provides means to convert the signal into the digital representation. It receives the signal from the thermocouple placed in the low temperature region of SETC and stores the information indicating it on the screen.
- 4.2 *CVRT – Thermocouple.* This function provides means to detect the temperature change in the low temperature region of SETC.
- 5.1 *CHNG – Furnace.* This function provides means to heat the steel shell up to temperature 850-900 °C. It has three indicators that show temperature in three spots of the cell surface: in the right hand side, in the middle, and in the left-hand side of SETC.
- 5.1.1 *CVRT- Resistance Heaters.* Resistance heaters are placed in the furnace to provide resistance to the current and heat up the SETC steel shell.
- 5.1.2 *CHNL – Conduction.* This function provides means to transfer the thermal energy from the furnace to the steel shell of SETC.
- 6.1 *STSP –Indicator.* This function provides means to convert the signal into the digital representation. It receives the signal from the thermocouple placed in the high temperature region of SETC and stores the information indicating it on the screen.

- 6.2 *CVRT – Thermocouple.* This function provides means to detect the temperature change in the high temperature region of SETC.
- 7.1 *CVRT – PC.* This function provides means to store measured data and assign the signals directed to electrode/electrolyte sample.
- 7.2 *CONN – Connection from PC to Frequency response analyzer (FRA) and potentiostat (PTST).* This function provides interface between PC and FRA and PTST. The connections should be properly checked to avoid parasitic losses.
- 7.3 *CVRT – Frequency response analyzer and potentiostat.*

This function provides means to apply and receive signals to and from the specimen. Solartron potentiostats feature two digital voltmeters with high accuracy and linearity throughout the instrumental range for simultaneous voltage and current measurement. They also offer 2, 3 and 4 terminal measurements. Coupled with a Solartron frequency response analyzer, such as the 1260 or 1255B, electrochemical impedance spectroscopy (EIS) measurements can be performed over a full 0.1Hz to 65kHz frequency range.

The Frequency Response Analyzer injects a test signal and measures the response of a system to that frequency on two return signals. It makes swept frequency response measurements that gives magnitude and phase data plotted verses frequency.

- 7.4 *CONN – Connection port.* This function provides interface among connection wires of FRA, PTST and contact board.
- 7.5 *BRCH – Contact board.* This function provides interface between leads from each electrode in SETC and leads of FRA and PTST.
- 8.1 *CHMG – Power Supply.* This function provides energy source to heat the sodium reservoir.
- 8.2 *CVRT-Heater Tape.* This function provides means to convert electricity into thermal energy in order to heat sodium reservoir to the temperature of 300 °C. The heater tape is banded around sodium reservoir and connected to the power supply.
- 8.3 *CHNL – Conduction.* This function provides means to transfer the thermal energy from the heater tape to the sodium reservoir.
- 9.1 *STSP – Ionization gage.* This function provides means to receive the signal from the pressure sensor converts and stores the information indicating it on the screen.
- 9.2 *CVRT – Pressure sensor.* This function provides means to sense the pressure change in SETC and convert that information to ionization gage indicator.

APPENDIX C
SETC FINITE ELEMENT MODELING

The Finite Element Approach to Thermal Analysis

Let's consider the two-dimensional heat conduction

$$\frac{\partial}{\partial x} \left(K_{xx} \frac{\partial T}{\partial x} \right) + \frac{\partial}{\partial y} \left(K_{yy} \frac{\partial T}{\partial y} \right) + Q = \rho c \frac{\partial T}{\partial t} \quad [38]$$

Since the SETC manifold is exposed to the ambient conditions there is convection on the surface of the manifold and steel tubes. Using Newton's law of cooling³⁴

$$q = h(T - T_{\infty}) \quad [39]$$

and conservation of energy and after some simplifications and rearrangements we can obtain the equation for two-dimensional heat conduction with convection as

$$\frac{\partial}{\partial x} \left(K_{xx} \frac{\partial T}{\partial x} \right) + \frac{\partial}{\partial y} \left(K_{yy} \frac{\partial T}{\partial y} \right) + Q = \rho c \frac{\partial T}{\partial t} + \frac{hP}{A}(T - T_{\infty}) \quad [40]$$

For steady state, any differentiation with respect to time is equal to zero, so equation [40] becomes³⁴

$$\frac{\partial}{\partial x} \left(K_{xx} \frac{\partial T}{\partial x} \right) + \frac{\partial}{\partial y} \left(K_{yy} \frac{\partial T}{\partial y} \right) + Q = \frac{hP}{A}(T - T_{\infty}) \quad [41]$$

The total potential energy functional is³⁵

$$\pi_h = U + \Omega_Q + \Omega_q + \Omega_h \quad [42]$$

$$\text{where } U = \frac{1}{2} \iiint_V \left[K_{xx} \left(\frac{\partial T}{\partial x} \right)^2 + K_{yy} \left(\frac{\partial T}{\partial y} \right)^2 \right] dV \quad [43]$$

$$\Omega_Q = - \iiint_V Q T dV \quad \Omega_q = - \iint_{S_2} q T dS \quad \Omega_h = \frac{1}{2} \iint_{S_3} h (T - T_\infty) \quad [44]$$

S_2 and S_3 are separate surface areas over which heat flow q and convection loss

$h(T - T_\infty)$ are specified.

After discretizing the continuum and selecting element type we select a temperature function

$$\{T\} = [N_i N_j N_m] \begin{Bmatrix} T'_i \\ T'_j \\ T'_m \end{Bmatrix} \quad [45]$$

where T'_i , T'_j , T'_m are the nodal temperatures, and the shape functions, which depends

on the number of nodes in the selected element, are given as

$$\begin{aligned} N_i &= \frac{1}{2A} (\alpha_i + \beta_i x + \gamma_i y) \\ N_j &= \frac{1}{2A} (\alpha_j + \beta_j x + \gamma_j y) \\ N_m &= \frac{1}{2A} (\alpha_m + \beta_m x + \gamma_m y) \end{aligned} \quad [46]$$

$$\begin{aligned} \text{where } \alpha_i &= x_j y_m - y_j x_m & \alpha_j &= x_m y_i - y_m x_i & \alpha_m &= x_i y_j - y_i x_j \\ \beta_i &= y_j - y_m & \beta_j &= y_m - y_i & \beta_m &= y_i - y_j \\ \gamma_i &= x_m - x_j & \gamma_j &= x_i - x_m & \gamma_m &= x_j - x_i \end{aligned} \quad [47]$$

The gradient matrix is defined as

$$\{g\} = \begin{Bmatrix} \frac{\partial T}{\partial x} \\ \frac{\partial T}{\partial y} \end{Bmatrix} \quad [48]$$

Substituting equation [45] in equation [48] we have

$$\{g\} = \begin{bmatrix} \frac{\partial N_i}{\partial x} & \frac{\partial N_j}{\partial x} & \frac{\partial N_m}{\partial x} \\ \frac{\partial N_i}{\partial y} & \frac{\partial N_j}{\partial y} & \frac{\partial N_m}{\partial y} \end{bmatrix} \begin{Bmatrix} T'_i \\ T'_j \\ T'_m \end{Bmatrix} \quad [49]$$

Rewriting equation [49] in compact matrix form, we have

$$\{g\} = [B]\{T'\} \quad [50]$$

where, $[B]$ is the rectangular matrix on the right side of equation [50]

$$[B] = \frac{1}{2A} \begin{bmatrix} \beta_i \beta_j \beta_m \\ \gamma_i \beta_j \beta_m \end{bmatrix} \quad [51]$$

The heat flux/temperature gradient relationship is now

$$\begin{Bmatrix} q_x \\ q_y \end{Bmatrix} = -[D]\{g\} \quad [52]$$

where the material property matrix is

$$[D] = \begin{bmatrix} K_{xx} & 0 \\ 0 & K_{yy} \end{bmatrix} \quad [53]$$

At this point we will derive the element conduction matrix substituting the equations

[45] – [53] into equation [43] and [44] and then using equation [42], π_n can be written in

matrix form as

$$\pi_h = \frac{1}{2} \iiint_V \{g\}^T [D] \{g\} dV - \iiint_V \{T\}^T [N]^T Q dV - \iint_{S_2} \{T\}^T [N]^T q dS + \frac{1}{2} \iint_{S_3} h \left[\{T\}^T [N]^T - T_\infty \right]^2 dS \quad [54]$$

Substituting equation [50] into equation [54] and using the fact that the nodal temperatures $\{T\}$ are independent of the general coordinates x and y , and can therefore be taken outside of the integrals,

$$\begin{aligned} \pi_h = & \frac{1}{2} \{T\}^T \iiint_V [B]^T [D] [B] dV \{T\} - \{T\}^T \iiint_V [N]^T Q dV - \\ & - \{T\}^T \iint_{S_2} [N]^T q dS + \frac{1}{2} \iint_{S_3} h \left[\{T\}^T [N]^T - T_\infty \right]^2 dS \\ & - \left(\{T\}^T [N]^T + [N] \{T\} \right) T_\infty + T_\infty^2 \int dS \end{aligned} \quad [55]$$

In the equation above, the minimization is most easily accomplished by explicitly writing the surface integral S_3 with $\{T\}$ left inside the integral. On differentiating equation [55] with respect to $\{T\}$, we obtain

$$\begin{aligned} \frac{\partial \pi_h}{\partial \{T\}} = & \iiint_V [B]^T [D] [B] dV \{T\} - \iiint_V [N]^T Q dV \\ & - \iint_{S_2} [N]^T q dS + \iint_{S_3} h [N]^T [N] dS \{T\} - \iint_{S_3} [N]^T h T_\infty dS = 0 \end{aligned} \quad [56]$$

Simplifying equation above, we obtain

$$\left[\iiint_V [B]^T [D] [B] dV + \iint_{S_3} h [N]^T [N] dS \right] \{T\} = \{f_Q\} + \{f_q\} + \{f_h\} \quad [57]$$

The force matrices have been defined by

$$\{f_Q\} = \iiint_V [N]^T Q dV \quad \{f_q\} = \iint_{S_2} [N]^T q dS \quad \{f_h\} = \iint_{S_1} [N]^T h T_\infty dS \quad [58]$$

where $\{f_Q\}$ - heat source

$\{f_q\}$ - heat flux

$\{f_h\}$ - convection

Since we are formulating element equations of the form $f = kT'$, we have the element conduction matrix for the heat – transfer problem given in equation [57] by

$$[k] = \iiint_V [B]^T [D][B] dV + \iint_{S_1} h [N]^T [N] dS \quad [59]$$

where the first and second integrals in equation [59] are the contributions of conduction and convection, respectively. The first integral of equation [59] (conduction portion) is defined by

$$[k_c] = \iiint_V [B]^T [D][B] dV = \iiint_V \frac{1}{4A^2} \begin{bmatrix} \beta_i & \gamma_i \\ \beta_j & \gamma_j \\ \beta_m & \gamma_m \end{bmatrix} \begin{bmatrix} K_{xx} & 0 \\ 0 & K_{yy} \end{bmatrix} \begin{bmatrix} \beta_i \beta_j \beta_m \\ \gamma_i \gamma_j \gamma_m \end{bmatrix} dV \quad [60]$$

Assuming constant thickness in the element and noting that all terms of the integrand of equation [60] are constant, we have

$$[k_c] = \iiint_V [B]^T [D][B] dV = T' A [B]^T [D][B] \quad [61]$$

The second integral of equation [59] (the convection portion) is defined by

$$[k_h] = \iint_{S_1} h [N]^T [N] dS \quad [62]$$

Multiplying the matrices in equation [62] we obtain

$$[k_h] = h \iint \begin{bmatrix} N_i N_i & N_i N_j & N_i N_m \\ N_j N_i & N_j N_j & N_j N_m \\ N_m N_i & N_m N_j & N_m N_m \end{bmatrix} dS \quad [63]$$

We obtain the total structure conduction matrix

$$[K] = \sum_{e=1}^N [k^{(e)}] \quad [64]$$

The global force matrix is the sum of all element heat sources, and is given by

$$\{F\} = \sum_{e=1}^N \{f^{(e)}\} \quad [65]$$

The global equations are then

$$\{F\} = [K]\{T\} \quad [66]$$

with the prescribed nodal temperature boundary conditions given by

$$T = T_S \quad \text{on the surface of the steel shell and manifold,}$$

$$q = 0 \quad \text{on insulated boundaries}$$

$$Q = 0 \quad \text{no internal heat generation}$$

$$-\left[K_{xx} \frac{\partial T}{\partial x} + K_{yy} \frac{\partial T}{\partial y} \right] = h(T - T_\infty) \quad \text{convection on the manifold and steel}$$

tubes.

This problem now is amenable to solution by the finite element method. The code used to solve this problem is ANSYS FEA package.³⁶ The procedure used while solving this problem with ANSYS is given below.

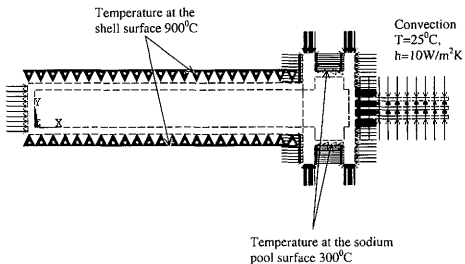


Figure 37. Thermal loading; condition (1)

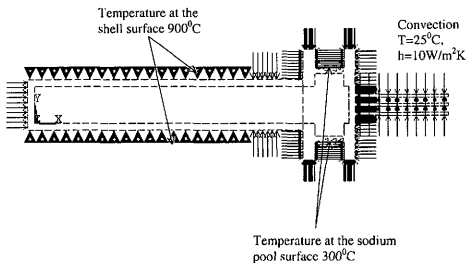


Figure 38. Thermal loading; condition (2)

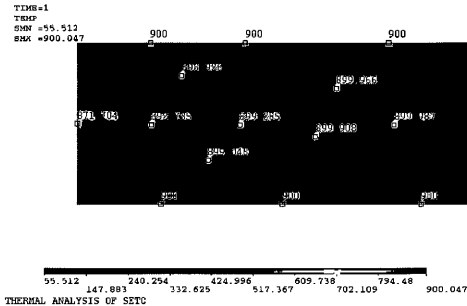


Figure 39. Temperature distribution at the hot end of SETC; condition (1)

Temperature gradients were observed in the sodium pool. The temperature distribution in the sodium pool is shown in the figure below.



Figure 40. Temperature distribution in the sodium pool; condition (1)

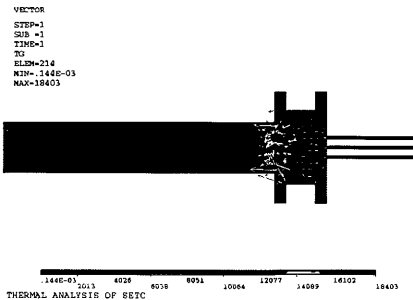


Figure 41. Vector plot of temperature gradients in SETC; condition (1)

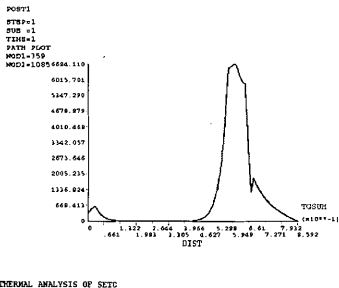


Figure 42. Graphical representation of the temperature gradients in SETC; condition (1)

PATH= THERPATH3
 VALUE= TEMP

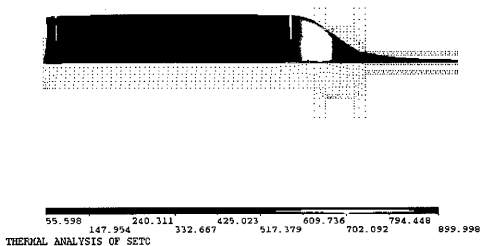


Figure 43. Representation of the temperature distribution on SETC geometry; condition (1)

PATH= THERPATH3
 VALUE= TGRAD

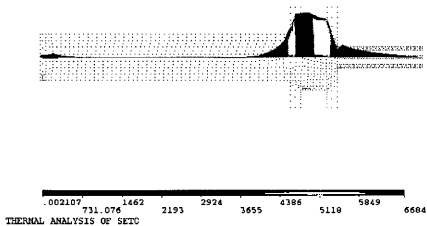


Figure 44. Representation of the temperature gradients on SETC geometry; condition (1)

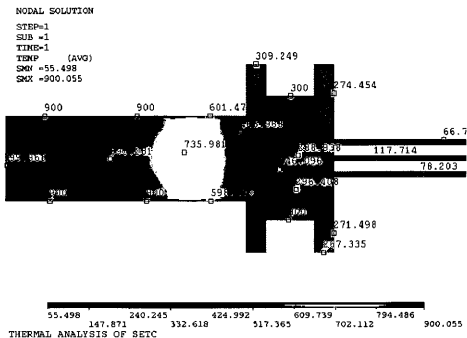


Figure 45. Temperature distribution in the sodium pool; condition (2)

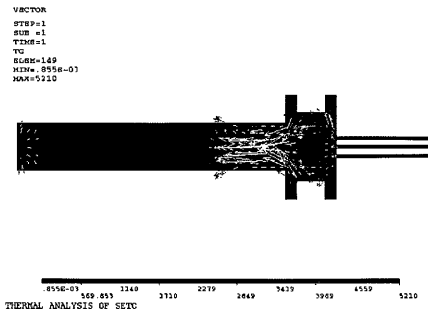
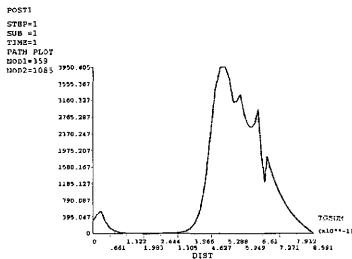


Figure 46. Vector plot of temperature gradients in SETC; condition (2)



THERMAL ANALYSIS OF SETC

Figure 47. Graphical representation of the temperature gradients in SETC; condition (2)

```

PATH= TEMPATH2
VALUE= TEMP

```

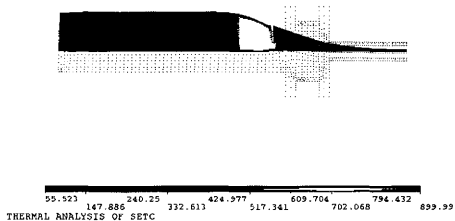


Figure 48. Representation of the temperature distribution on SETC geometry; condition (2)

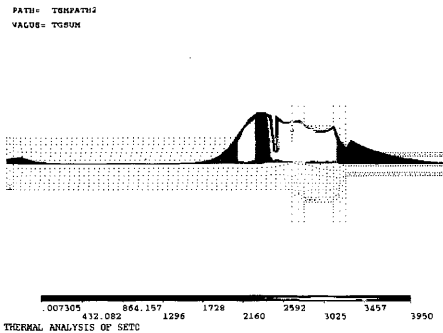


Figure 49. Representation of the temperature gradients on SETC geometry; condition (2)

APPENDIX D
SODIUM VAPOR PRESSURE CORRELATIONS

Roger Williams correlation (JPL)

$$P_{Na} = \frac{P_1(T_{Na} - 350)}{400} + \frac{P_2(750 - T_{Na})}{400} \quad [67]$$

where Ditchburn and Gilmour correlation³¹ is

$$P_1 = 101325 * 10^{(6.354 - \frac{5567}{T} - \frac{1}{2} \log T)} \quad [68]$$

and Buck and Pauly correlation³¹

$$P_2 = 133.3 \left(\exp(8.08 - \frac{5479}{T}) \right)^{\frac{1}{0.4343}} \quad [69]$$

Borgstedt correlation³⁷

$$P = 0.001 * \left(\exp \left(10.182516 - \frac{5693.8776}{T} + 0.000085874946 * T \right) * T^{0.4755} \right)^{\frac{1}{0.4343}} \quad [70]$$

Fischer correlation³⁸

$$P = 100 * \left(\exp \left(7.5087 - \frac{5342.3}{T} \right) \right)^{\frac{1}{0.4343}} \quad [71]$$

Walters et al. Correlation³⁹

$$P = 101325 * \left(\exp \left(4.6702 - \frac{5400}{T} \right) \right)^{\frac{1}{0.4343}} \quad [72]$$

Gordon et al. Correlation⁴⁰

$$P = 101325 * \left(\exp \left(8.4437 - \frac{5702}{T} \right) * T^{-0.51} \right)^{\frac{1}{0.4343}} \quad [73]$$

Makansi et al. Correlation⁴¹

$$P = 101325 * \left(\exp \left(4.521 - \frac{5220}{T} \right) \right)^{\frac{1}{0.4343}} \quad [74]$$

Stone et al. Correlation³¹

$$P = 101325 * 10^{\left(6.6808 - \frac{5544.41}{T} - 0.61344 * \log T \right)} \quad [75]$$

AMPS correlation

$$P = 101325 * 2.718265^{\left(14.631 - \frac{12818}{T} - 0.5 * \log T \right)} \quad [76]$$

Potter et al. Correlation³³

$$P = 10^6 * \left(\exp \left(11.2916 - \frac{12532.694}{T} \right) * T^{-0.3869} \right) \quad [77]$$

Bonilla et al. Correlation⁴²

$$P = 10^6 * \left(\exp \left(11.9463 - \frac{12633.73}{T} \right) * T^{-0.4872} \right) \quad [78]$$

Average calculated correlation

$$P = \frac{1}{2} * \left(16 * 10^9 * \frac{1}{\exp \left(\frac{12615}{T} \right)} + 1.54 * 10^{11} * T^{-0.5288} * \frac{1}{\exp \left(\frac{12633.73}{T} \right)} \right) \quad [79]$$

APPENDIX E

DERIVATION OF THE NORMALIZED EXCHANGE CURRENT DENSITY (B)

The following section shows the derivation of the normalized exchange current density from measured quantities in an SETC experiment. It is a condensed version of the derivation by Williams, et al. presented in references 9 and 16.

The apparent charge transfer resistance, R_{act} , is defined as

$$R_{act} = - \left(\frac{dE}{dj} \right)_T \quad [80]$$

where E is the cell potential and j is the cell current. E and j are related by the current-overpotential equation, equation [81], which is written to include the contributions of the interfacial and bulk sodium pressure, and the interfacial and bulk sodium ion concentrations.

$$j = J_o \cdot \frac{(P_{el} e^{-\alpha E f} - P_{Na} e^{(1-\alpha) E f})}{P_{el} + K_f J_o e^{(1-\alpha) E f}} \quad [81]$$

where

$$J_o = J_o \left(\frac{P_{el}}{P_{Na}} \right)^\alpha \quad \text{and} \quad \eta = E - \frac{1}{f} \ln \frac{P_{el}}{P_{Na}} \quad [82]$$

J_e is the standard exchange current density at the actual equilibrium potential of the cell, while J_e^* is the exchange current density at an equilibrium potential with saturated sodium vapor in contact with the electrode.

Differentiating equation [81] with respect to E and inverting results in equation [83] when both $\eta=0$ and $j=0$, representing open-circuit conditions.

$$R_{act} = \frac{RT_{el}}{FJ_e} + \frac{K_f RT_{el}}{FP_{Na}} \quad [83]$$

At extremely low magnitude AC currents, the second term can be neglected reducing the equation to

$$R_{act} = \frac{RT_{el}}{FJ_e} \quad [84]$$

The normalized exchange current density, B , is defined as the standard exchange current density, J_e , normalized to the sodium collision rate and reaction rate at unit activity sodium and is shown in equation [85].

$$B = \frac{J_e^* \sqrt{T_{el}}}{P_{el}} \quad [85]$$

Using equations [82] in equation [85], an expression relating B directly to R_{act} is obtained.

$$B = \left[\frac{T_{el}}{P_{el} P_{Na}} \right]^{1/2} \left[\frac{RT_{el}}{R_{act} F} \right] \quad [86]$$

VITA

Ulughbek Bakhadirovich Azimov was born in the city of Andijan, Uzbekistan on July 30, 1972. He graduated with honors with a Bachelor of Science degree in mechanical engineering from Andijan Technical University in July 1996. He worked as a design engineer in the Uzbek-South Korean Joint Venture UZ-DAEWOO auto automobile-producing company from 1996 to 1998. In 1998 he received a scholarship of the president of Uzbekistan that allowed him to gain knowledge at a U. S. university, in particular at Texas A&M University in College Station. In December 2001 he obtained a Master of Science degree in mechanical engineering from Texas A&M University.

Ulughbek B. Azimov worked in the Center for Space Power, which is a research institution affiliated with Texas A&M University, as a graduate research assistant from April 2000 to December 2001. His research experience and interests include work in the area of Alkali Metal Thermal to Electric Conversion (AMTEC).

The permanent address where he may be reached is 1 Haydarov St., Andijan, Uzbekistan, 710000, tel: (011998) 742-24-31-26, e-mail: uazimov@hotmail.com.